Available online at www.sciencedirect.com

ScienceDirect

Geochimica et Cosmochimica Acta 126 (2014) 228–249

Geochimica et Cosmochimica Acta

www.elsevier.com/locate/gca

Selenium redox cycling during weathering of Se-rich shales: A selenium isotope study

Jian-Ming Zhu [a,b,*], Thomas M. Johnson [b,1], Scott K. Clark [c], Xiang-Kun Zhu [d], Xiang-Li Wang [b]

[a] *The State Key Laboratory of Environmental Geochemistry, Institute of Geochemistry, Chinese Academy of Sciences, No. 46 Guanshui Road, Guiyang 550002, China*

[b] *Department of Geology, University of Illinois at Urbana-Champaign, Urbana, IL 61801, USA*

[c] *Department of Geology, University of Wisconsin-Eau Claire, Eau Claire, WI 54702, USA*

[d] *The Key Laboratory of Isotopic Geology, The Ministry of Land and Resources, Institute of Geology, Chinese Academy of Geological Sciences, Beijing 100037, China*

Received 20 September 2012; accepted in revised form 6 November 2013; available online 20 November 2013

Abstract

Selenium isotopes are becoming an important paleoenvironmental proxy. However, few studies have focused on the behavior of Se isotopes during oxidative weathering. In this paper, a comprehensive set of Se isotopic composition and concentration data were collected from the weathering profiles of Se-rich shales of the Permian Maokou Formation in Yutangba and Shadi, China to investigate Se isotopic fractionation and Se enrichment during weathering processes. The $\delta^{82/76}$Se in fresh shales (148 ± 118 mg/kg Se, 1SD, $n = 40$) from Shadi and Yutangba drill cores varies from $-1.69‰$ to $1.74‰$ with an average of $0.40 \pm 0.71‰$ (1SD, $n = 40$), consistent with the range in other Phanerozoic shales, suggesting that Se isotopes are not strongly fractionated during Se sequestration in the primary sedimentary environment. However, the strongly weathered Se-rich shales from Shadi and Yutangba profiles are isotopically lighter with average $\delta^{82/76}$Se values of $-1.96 \pm 1.08‰$ (1SD, $n = 5$) and $-1.08 \pm 1.83‰$ (1SD, $n = 23$), respectively. These data suggest that Se isotopes can be fractionated during oxidation and reduction processes associated with weathering, with heavier isotopes removed preferentially during oxidative weathering of shales. Such a shift, if found to be a global phenomenon, would have implications for models of the global Se cycle and interpretation of Se isotope data from past biogeochemical regimes.

Locally altered shales exposed in a quarry at Yutangba are extremely enriched in Se with 1642 ± 1505 mg/kg (1SD, $n = 45$), approximately 10 times greater than that in unaltered drill core samples. These rocks display very strong variation in $\delta^{82/76}$Se over short distances, with a single 60 cm transect showing the most strongly negative and positive $\delta^{82/76}$Se values ($-14.20‰$ to $+11.37‰$) observed to date in natural samples. This suggests that Se has undergone multiple cycles of oxidation, mobilization, and re-reduction, resulting in a Se-rich redox front that has migrated downward through the organic-rich shales over time. $\delta^{82/76}$Se values vary sharply over distances as small as 10 cm, indicating that Se redox conditions change strongly with position and are controlled by fractures and rock layering. Our data and a simple conceptual model suggest that zones of increased permeability that are accessed first by infiltrating waters are isotopically light, whereas less accessible zones are heavy. Repeated redox cycling accentuates this pattern. Furthermore, the average $\delta^{82/76}$Se in Se-rich shales at the Yutangba weathering system is $0.45 \pm 5.77‰$ (1SD, $n = 39$), identical with that ($0.40 \pm 0.71‰$) in fresh shales from same locality, implying that Se released by weathering accumulates in the redox front with little loss. The strong Se isotopic fractionation

* Corresponding author at: The State Key Laboratory of Environmental Geochemistry, Institute of Geochemistry, Chinese Academy of Sciences, No. 46 Guanshui Road, Guiyang 550002, China. Tel.: +86 851 5895787; fax: +86 851 5891609.

E-mail addresses: zhujianming@vip.gyig.ac.cn (J.-M. Zhu), tmjohnsn@illinois.edu (T.M. Johnson).

[1] Tel.: +1 217 2442002; fax: +1 217 2444996.

0016-7037/$ - see front matter © 2013 Elsevier Ltd. All rights reserved.

http://dx.doi.org/10.1016/j.gca.2013.11.004

occurring in the redox front implies that Se isotopes can be extensively used in tracing geochemical processes of Se in groundwater system, especially related to fractures.
© 2013 Elsevier Ltd. All rights reserved.

1. INTRODUCTION

Selenium (Se) is an essential trace element for human beings and animals, but is toxic at high concentrations (WHO, 1987; Rayman, 2000; Lens and Lenz, 2009). The distribution of Se on the earth's surface varies widely, forming both Se-excessive and Se-deficient geo-ecosystems where human and animal health problems are well documented (Yang et al., 1983; Presser et al., 1994; Zheng et al., 1999; Tan et al., 2002; Fordyce, 2007). The weathering of sedimentary rocks, particularly in Se-rich shales, leads to most Se contamination problems worldwide (Zhu et al., 2008a; Lens and Lenz, 2009). Furthermore, Se isotopes in black shales are becoming a powerful paleo-oceanographic proxy that could provide information about past redox changes in earth systems, from the great oxygenation event to Phanerozoic oceanic anoxic events (Mitchell et al., 2012). Consequently, selenium has received considerable attention in geological, environmental, biological and agricultural sciences (Rouxel et al., 2002, 2004; Zhu et al., 2008b, 2009; Lens and Lenz, 2009; Williams et al., 2009; Clark and Johnson, 2010; Fairweather-Tait et al., 2011; Wen and Carignan, 2011; Mitchell et al., 2012).

Selenium is a redox-sensitive element, as it can occur in the -II, 0, IV, and VI oxidation states in natural environments (Elrashidi et al., 1987; Seby et al., 2001). Selenate, referred to below as Se(VI), is highly soluble, mobile and bioavailable. Selenite and hydroselenite, referred to below as Se(IV), are also highly soluble, but tend to adsorb onto organic matter, clay minerals and oxide minerals. Elemental Se, Se(0), is readily precipitated, sparingly soluble and less mobile. Selenides (Se(-II)) can exist in insoluble metal-selenide and metal-sulfide minerals, or as organic Se compounds formed by assimilatory biological reduction of Se (Howard, 1977; Balistrieri and Chao, 1990; Nelson et al., 1996; Seby et al., 2001; Johnson, 2004; Kulp and Pratt, 2004; Stolz et al., 2006). Thus, the mobility, bioavailability, and toxicity of Se vary greatly depending on its oxidation state. Additionally, Se is an important micronutrient, and organically bound Se (org-Se) is an important constituent in many systems. Selenium cycling in wetland sediments is dominated by org-Se fluxes (Clark and Johnson, 2010). In the modern oceans, Se exhibits nutrient-like profiles, suggesting that a large fraction of the total Se may be present as org-Se and sulfide/selenide-Se in organic-rich shales that formed under dysoxic conditions (Cutter and Bruland, 1984; Cutter and Cutter, 1995; Kulp and Pratt, 2004; Zhu et al., 2012).

Because of the complex geochemistry of Se, its behavior in the critical zone (soils and weathering horizons) is both complex and poorly understood. A better understanding of Se fluxes and chemical transformations is needed to enable better prediction of the processes that lead to either Se deficiency or Se toxicity in various environments. Furthermore, Se could be useful as an indicator of redox conditions that affect other processes such as U(VI) or As(V) reduction. A better understanding of geochemical processes affecting Se in weathering environments would aid in a range of scientific investigations.

Precise measurements of Se isotope ratios provide a new means to examine Se redox processes. Recently, Se isotopes, like those of several other heavier elements (Bullen and Eisenhauer, 2009; Bullen and Walczyk, 2009), have been developed as new geochemical tools that can be applied in environmental, agricultural, life and biomedical research (Herbel et al., 2002; Johnson and Bullen, 2004; Chanton et al., 2008; Zhu et al., 2008a; Clark and Johnson, 2010; Mitchell et al., 2012). Selenium has six naturally occurring stable isotopes, ^{74}Se, ^{76}Se, ^{77}Se, ^{78}Se, ^{80}Se, and ^{82}Se, whose abundance are 0.89%, 9.37%, 7.64%, 23.77%, 49.61%, and 8.73%, respectively. Following the pioneering work of Krouse and Thode (1962), recently developed methods have exploited negative ion thermal ionization mass spectrometry (TIMS) and hydride generation (HG)-multicollector inductively coupled plasma-mass spectrometry (MC-ICP-MS) to produce precise and accurate measurements of Se isotope ratios using as little as 20 ng Se (Johnson et al., 1999; Rouxel et al., 2002; Carignan and Wen, 2007; Zhu et al., 2008a). External reproducibilities of $\pm 0.1‰$ (2σ) for clean reference materials (NIST SRM 3149 and MH 495) and less than $\pm 0.2‰$ (2σ) for natural samples have been obtained using a $^{74}Se + {}^{77}Se$ double-spike technique combined with HG-MC-ICP-MS (Zhu et al., 2008a). These analytical techniques have greatly improved the efficiency of Se isotope measurement and broadened Se isotope applications for those natural samples with low Se concentration.

Selenium isotopes can be fractionated by equilibrium and kinetic processes (Krouse and Thode, 1962; Johnson, 2004; Li and Liu, 2011). Li and Liu (2011) estimated isotopic fractionation factors ($\alpha = R_a/R_b$, where R is the isotope ratio) that would result from isotopic equilibrium between different Se oxidation states. They estimated $\alpha \approx 1.0134$ for SeO_4^{2-}–SeO_3^{2-} equilibrium at 25 °C, and showed a general trend of heavy Se isotope enrichment in the order $SeO_4^{2-} > SeO_3^{2-} > HSeO^{3-} > SeO_2 >$ selenoamino acids > alkylselenides > Se(0) or $H_2Se > HSe^-$.

A variety of experiments have sought to determine isotopic fractionation factors for kinetically controlled reactions. Selenium isotope fractionation has been found to result from both biological and abiotic processes (Rees and Thode, 1966; Herbel et al., 2000; Rouxel et al., 2002; Johnson, 2004), and a preliminary assessment of Se isotope systematics has been constructed (Johnson et al., 1999; Johnson, 2004; Johnson and Bullen, 2004). Large Se isotope fractionations have been found during reduction of Se oxyanions, during which reaction products are enriched in lighter isotopes, whereas the unreduced fraction becomes

isotopically heavier as reduction proceeds. The largest fractionations have been observed during abiotic reduction of Se(VI) to Se(0) by green rust ($\alpha \approx 1.0112$) and dissimilatory reduction of Se(VI) to Se(0) in pure cultures of microbes ($\alpha \approx 1.0089$–1.0112) (Herbel et al., 2000; Johnson and Bullen, 2003). In comparison with these reactions, other processes such as oxidation of reduced Se, adsorption by Fe oxides and assimilation by plants or algae, are associated with smaller isotopic fractionation of less than 4.2‰ (Johnson and Bullen, 2004; Clark and Johnson, 2010; Schilling et al., 2011). Using the emerging knowledge of these systematics, Se isotopes have been used as tracers of pollution sources, occurrence and extent of Se redox reactions, and biogeochemical processes in a variety of modern environments and ancient environments, including shales, soils, sediments, ground waters, rivers, lakes and wetland areas (Herbel et al., 2002; Rouxel et al., 2004; Carignan and Wen, 2007; Clark and Johnson, 2008, 2010; Wen and Carignan, 2011; Mitchell et al., 2012).

Variations in Se isotope ratios in weathering profiles have not been studied extensively, despite the successful application of lithium and molybdenum isotope data in weathering studies (Duan et al., 2010; Pearce et al., 2010; Teng et al., 2010). Variations of Se isotope ratios in various geological reservoirs have been reported in Johnson (2004), Rouxel et al. (2002), Carignan and Wen (2007) and Clark and Johnson (2010). $\delta^{82/76}$Se (see Eq. (1)) values of meteorites and basalts are close to zero relative to the NIST SRM-3149 reference solution, with mean values of 0.01 ± 0.32‰ (1SD, $n = 4$) and 0.38 ± 0.71‰ (1SD, $n = 4$), respectively, suggesting the bulk earth should be close to zero. However, Se isotopes in weathered shales display a very large variation of $\delta^{82/76}$Se of more than 17‰, suggesting that weathering processes related to Se redox transformations may lead to significant Se isotopic fractionation in surficial environments (Johnson, 2004; Zhu et al., 2008a; Wen and Carignan, 2011). However, data are still sparse at present and more work must be done to investigate the systematics of Se isotopic fractionation during weathering processes of sedimentary rocks, particularly in Se-rich shales, which are the sources of most Se contamination problems worldwide.

Enshi Prefecture is one of several areas in China where Se-rich rocks and soils occur. In the village of Yutangba, a sudden incidence of human Se poisoning took place in 1963 (Yang et al., 1983; Zheng et al., 1999). Previous studies have shown that Se was mainly sourced from the carbonaceous shale and carbonaceous chert of the Lower Permian Maokou and Wujiaping Formations (Yao et al., 2002; Zhu et al., 2008b; Wen and Carignan, 2011). The Se concentrations in these strata are high and variable. Several kinds of Se minerals such as native Se and krutaite ($CuSe_2$), and Se concentrations greater than 3% were found in some of Yutangba's shale layers (Zhu et al. 2004, 2012). These strata were investigated as a potentially useful Se ore deposit in 1987 (Song, 1989). Wang and Li (1996) suggested that the formation of this deposit occurred because of its nearly vertical bedding, combined with the processes of oxidation, leaching and adsorption of Se by organic matter. However, the primary rock, prior to weathering, was already Se-rich. Yao et al. (2002) suggested that primary Se-rich shales were formed in a shallow sea transitioning to a moderately deep anoxic environment, and the Se enrichment was mainly controlled by biological processes. Those studies suggested that Se enrichment in Yutangba occurred as a result of both primary and secondary processes. However, those models do not allow one to distinguish between the various potential mechanisms of Se enrichment.

Wen and Carignan (2011), in a study of three Se-bearing ore deposits in China, presented a suite of $\delta^{82/76}$Se data from the Yutangba rocks. Nine whole rock samples, six kerogen extracts, and two soil samples revealed a wide range in $\delta^{82/76}$Se from -12.9‰ to 7.5‰. Accordingly, they suggested that redox-driven Se redistribution in a weathering environment is favorable to explain the formation of the Se ore deposit in Yutangba and the occurrence of native Se. Their study, and sparse data from other Se isotope studies of weathered materials (Hagiwara, 2000; Clark and Johnson, 2010) suggest that Se isotope should be useful indicators of redox processes in weathering environments.

The present study was designed to examine in detail the systematics of Se redistribution, and the accompanying Se isotope ratio shifts, as Se-rich shales are weathered. The Se-rich shales of Enshi Prefecture were chosen because the history of human and animal Se poisoning drives a practical necessity to determine precisely the patterns and mechanisms of Se enrichment, and also because the high Se concentrations allow relatively easy sample preparation. Systematic, dense sampling of the rock outcrops and soils was conducted to obtain a large suite of samples that reveals the small scale variability, the moderate-scale mean values, and larger scale trends of Se concentration and $\delta^{82/76}$Se. Samples of water and water-deposited minerals were collected to determine the composition of mobilized Se. Archived drill core samples, from depths as great as 274 m below the ground surface, were obtained with the goal of determining the primary composition of the rock prior to any weathering and providing conclusive proof that the $\delta^{82/76}$Se variations observed by Wen and Carignan (2011) were not primary features of the rock. Samples from a wide range of depth were obtained so that the transition from the weathering zone to the fresh rock could be observed.

The resulting detailed, systematic data set reveals the range of primary Se concentrations and $\delta^{82/76}$Se values in the Enshi rocks, and provides deeper insights into the systematics of Se remobilization in shale weathering zones. This leads to a preliminary understanding of $\delta^{82/76}$Se values of soluble Se exported from weathering rocks, which is needed to define isotopic fluxes in the global Se cycle. This information is needed for studies using $\delta^{82/76}$Se measurements in ancient marine sediments as indicators of past marine redox shifts. Furthermore, the present study provides information regarding the fidelity of outcrop samples as indicators of primary rock composition and the depth to which alteration can persist.

2. GEOLOGICAL SETTING AND SAMPLING

The Lower Permian Maokou (P_1m^3) formation in Enshi Prefecture, also named as "Gufeng formation" elsewhere

(Yao et al., 2002; Kametaka et al., 2005), is notorious in China for Se enrichment, and mainly consists of carbonaceous shale and carbonaceous chert (Finkelman et al., 1999; Zheng et al., 1999; Yao et al., 2002). The formation is widely exposed in southwest Hubei Province (Fig. 1A). The Se-rich strata in Yutangba are located in the northwestern limb of the Shuanghe syncline (Fig. 1B), in the northeastern part of the Upper Yangtze Platform fold belt (Wang and Li, 1996; Yao et al., 2002; Wen and Carignan, 2011), approximately 81 km SE of Enshi City (Fig. 1A, 30°10′810″N, 109°46′728″E). These strata strike ENE and dip 45–70° SSE (Fig. 1C). Several SSE-dipping normal faults were developed within the strata (Figs. 1C and 2). The Se-rich strata (30°20′304″N, 109°45′124″E) in Shadi of Enshi are stratigraphically similar to those in Yutangba, but are nearly horizontal.

The Se-rich strata generally consist of a suite of black, thin-layered carbonaceous chert interbedded with carbonaceous shale, about 10 m in thickness. The rock is extremely rich in organic carbon, ranging from 3.7% to 46.6% with an average of 17.1 ± 10.7% (1SD, $n = 24$); these rocks are locally known as stone coal, which are unmetamorphosed and show no evidence of hydrothermal alteration. Several thin-layered tuffs with 0.5–1 cm thicknesses within shale were found in this study; these were either present as calcareous tuff or altered to mudstone. The chert layers are commonly 3–11 cm in thickness and exhibit massive, laminated structures. The shales are 2–8 cm in thickness and also exhibit laminated structures.

The steeply dipping Yutangba section contains such high Se concentrations that it has been described as an ore deposit. Several such deposits are thought to be present locally as lenticular bodies (Fig. 1C), associated with normal faults, ranging roughly from 30 m to 150 m in length, from 0.7 m to 5.2 m in thickness, and from 14 m to 35 m in depth (Wang and Li, 1996; Yao et al., 2002). Selenium minerals such as krutaite ($CuSe_2$), klockmannite (CuSe), and native Se were found there (Wang and Li, 1996; Zhu et al., 2004, 2012).

Rock samples spanning a range of weathering intensity were collected at Yutangba and Shadi. The samples are categorized as weakly weathered, strongly weathered, or fresh, depending on observations of hand specimens and their locations (depth) relative to the original ground surface prior to quarrying. At Shadi, three groups of samples were collected from a newly cut vertical profile (13 m height) in 2003 and 2006, within a hillside quarry exposing the nearly horizontal strata. Four fresh samples (labeled with the prefix SD), were collected near the bottom of the profile. These samples are uniformly solid black in color, whereas the

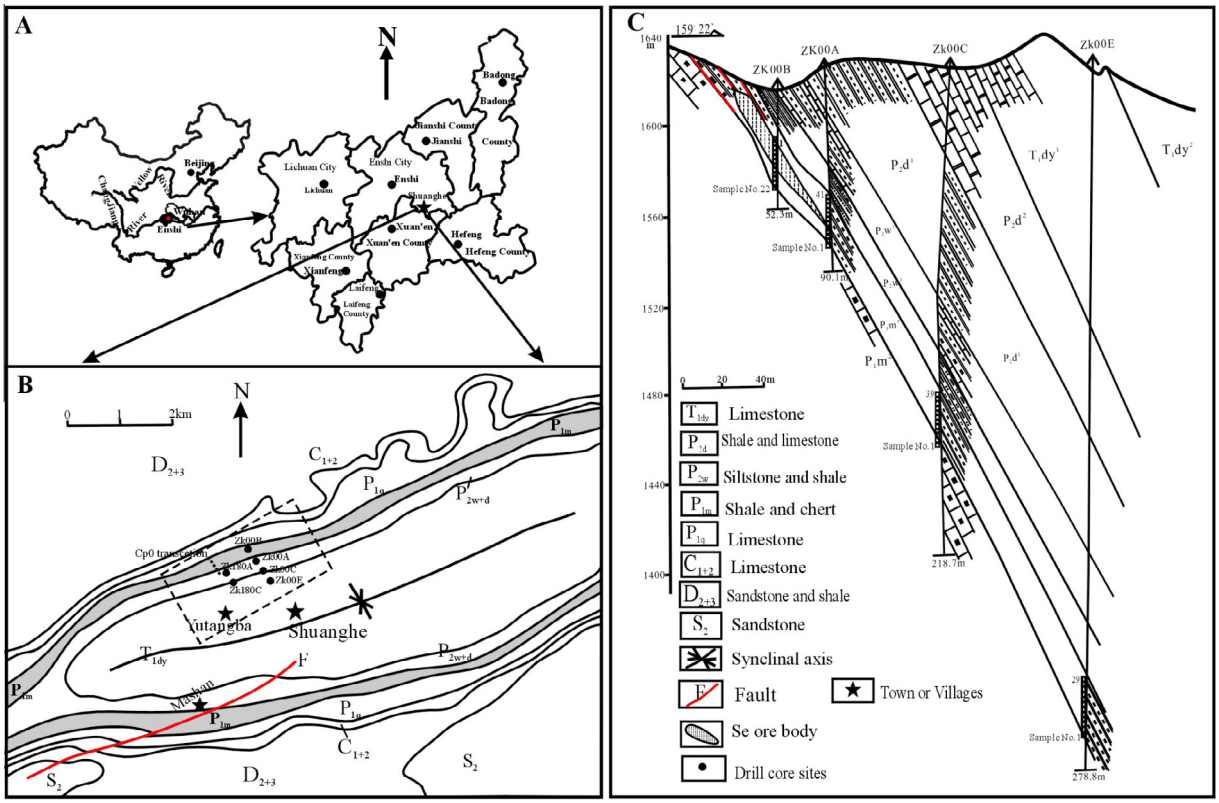

Fig. 1. Geological sketch map showing sampling and drill core locations at Yutangba, Enshi, China. (A) Sketch map showing the location of Enshi Prefecture in China. (B) The geological map showing the distribution of Se-rich rocks' strata and the site of drill cores at Yutangba. (C) The cross section showing sampling locations and their depth at Yutangba. T_1dy: Lower Triassic (Daye formation); P_2d and P_2w: Middle Permian (Wujiaping and Dalun formation); P_1m: Lower Permian (Maokou Formation); P_1q: Lower Permian (Qixia Formation); C_{1+2}: Middle-Lower Carboniferous; D_{2+3}: Middle-Upper Devonian; S_2: Middle Silurian.

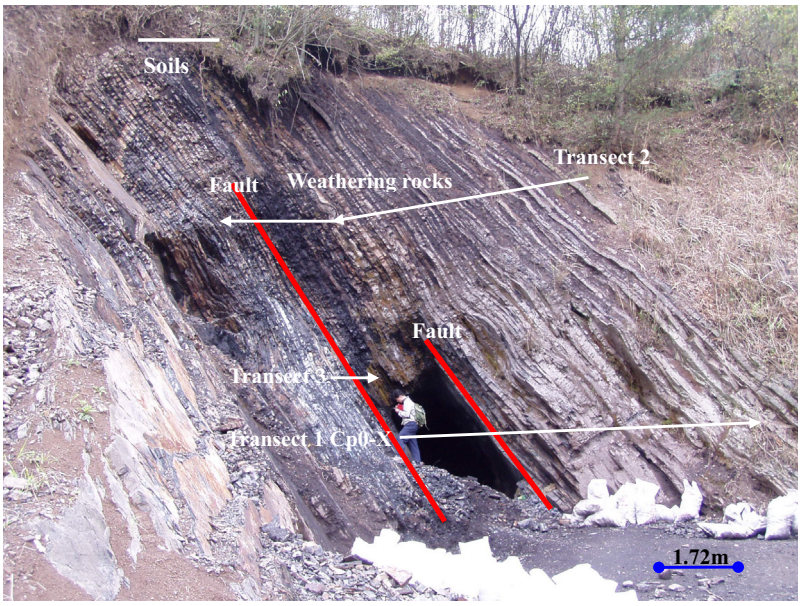

Fig. 2. Photo of the quarry face at Yutangba, showing the layering of the rock and the locations of sampling transects.

weakly weathered rocks show sparse iron staining and/or lighter colors on fracture surfaces, and the strongly weathered rocks are softer, lighter in color, and laden with iron oxides. Strongly weathered rocks were found near the top of the outcrop; 5 samples (labeled using the SDIII prefix) were taken. Eight weakly weathered samples (SDI prefix) were collected from the middle of the profile. One sample of water seeping from the quarry face near the profile, and two efflorescent salt samples, were also collected.

At Yutangba, where the same strata are inclined steeply, samples were collected along a series of transects traversing horizontally across the strata exposed in a quarry face (Fig. 2). Transect 1 (Cp0 prefix) consisted of 24 mildly altered samples collected about 2 m above the quarry floor in 1997, with roughly 0.1 m spacing between samples. Transect 2 (Ytb prefix) sampled strongly weathered samples several meters above the quarry floor at about the same spacing in 2006. Transect 3 (Ytb- prefix) consisted of closely spaced samples taken along a line 50 cm in length, very close to transect 1, about 2 m above the quarry floor. Transects 1 and 3 transected two faults that appear to have created weaknesses and possibly conduits for fluid flow in the rock. Finally, four samples of the soils developed at the top of the outcrop were collected in 2006 (Fig. 2). One seep water sample was taken from a short adit created for ore exploration purposes. All rock samples were trench-cut, generally 1 kg in weight and sealed in polyester plastic bags for transport. Wet samples were freeze-dried soon after they were taken back to the laboratory.

Drill core samples, taken in 1987 by the No. 4 Geological party of Hubei, were also obtained; these were fresh or slightly altered. The samples were mainly from drill holes Zk00A, Zk00B, Zk00C,Zk00E, Zk180A, Zk180C, but a few came from other sites. These samples were powdered and stored in a sealed vessel closely packaged with polyester plastic bags. Drill core locations are shown in Fig. 1B and C. Of these, Zk180A and Zk180C are directly down-dip from the sampled quarry face, while Zk00A, B C and E are located several hundred meters to the NE (Fig 1C).

3. ANALYTICAL METHODS

3.1. Sample digestion

Rock samples were digested using a mixed acid solution in high pressure Parr® digestion vessels. Typical masses of powder were 50–100 mg; these were weighed into 23 ml PTFE bomb liner vessels. To each sample 0.5 ml concentrated HF (38%) and 0.5 ml HNO_3 (15.6 M) was added; the solution was allowed to decompose carbonate minerals at room temperature for 2 h. Then, 2.2–2.5 ml of HNO_3 was added. The Parr bombs were sealed and placed in a pre-heated oven for 16 h at 155 ± 5 °C. After cooling, 1–2 ml of 30% H_2O_2 was added, and the liner was allowing to stand, covered on a hot plate at 70 °C for about 1 h. The clear solution was transferred to 15 ml Savillex beakers and taken to incipient dryness at 70 °C. The residue was redissolved by adding 1 ml of 7.8 M HNO_3, then diluted with Milli-Q water to attain 5 ml of sample stock solution. Because Se concentrations in our samples were very high and ranged from 2 mg/kg to 3%, small aliquots of 0.2–1 ml solution were used for the Se concentration and isotope measurements. These aliquots, after addition of 0.5 or 1 ml HNO_3, were evaporated to incipient dryness, and then dissolved in 5 ml of 5 M HCl. These solutions were heated for 60 min in glass tubes with Teflon caps at 100 °C in aluminum blocks, then diluted with MQ-water to 30 ml (0.83 M HCl) or 12.5 ml (2 M HCl) for Se concentration measurement by hydride generator-atomic fluorescence spectrometry (HG-AFS) (Zhu et al., 2008b) or

MC-ICP-MS. Duplicates, reagent blanks and standard solutions (NIST SRM3149 and MH495) were treated exactly as were the samples. Total sulfur (TS) in samples was measured by an element analyzer (Elementar Vario Macro Cube), Total organic carbon (TOC) was also determined using an element analyzer (Elementar Vario Macro Cube) after treatment of the sample with 1 M HCl to remove carbonate. The measured TS and TOC in standard USGS SGR-1b were 1.59 ± 0.07 wt% (1SD, $n = 6$) and 24.9 ± 0.20 wt/% (1SD, $n = 8$), respectively, which are consistent with the certified values of 1.53 ± 0.11 wt/% and 24.8 wt/%. Total iron (TFe) was determined using inductively coupled plasma-optical emission spectrometry (ICP-OES) after treatment of sample digestion by Parr bomb; the average Fe concentration in standard USGS SGR-1b were determined to be 2.15 ± 0.09 wt% (1SD, $n = 6$), which is in agreement with the certified concentration of 2.12 ± 0.10 wt/%. Titanium (Ti) concentrations were determined by ELAN DRC-e ICP-MS at The Institute of Geochemistry, CAS, with Rh as an internal standard (Liang et al., 2000). These results are reported on a bulk-rock basis and the relative standard deviation (RSD) is less than 10%.

3.2. Chemical separation with TCF

Previous studies have shown that thiol cotton fiber (TCF) can be successfully used in chemical separation of Se from the sample matrix (Marin et al., 2001; Rouxel et al., 2002; Elwaer and Hintelmann, 2008). Before the separation procedure, a double isotope tracer solution (see below) was added. The procedure in this study was similar to that described in Rouxel et al. (2002). However, some modifications have been made to remove residual organic compounds that appeared to interfere with Se isotope measurements (Zhu et al., 2008a). We present here a brief summary: The sample, in 5 ml of 5 N HCl, is diluted to 30 ml to load onto 10 ml polypropylene columns filled with 0.14 g of TCF, previously washed with 3 ml H_2O and conditioned with 1 ml 6 N HCl and 1 ml 0.8 N HCl. The TCF column was rinsed with 2 ml of 6 N HCl, followed by 3 ml H_2O. The TCF was suctioned to dry it and transferred to a 15 ml centrifuge tube. 1 ml of a well-mixed solution of $HNO_3 + 30\%$ $H_2O_2 + H_2O$ was injected into the tube, which was suspended in a boiling-water bath for 20 min to completely desorb Se. 3.5 ml H_2O was added and the TCF was centrifuged for 20 min. The supernatant was decanted into a 15 ml Savillex beaker and evaporated to a small spot (100 µl), then treated with a mixed solution of HNO_3 and H_2O_2 several times until a colorless tiny spot less than 5 µl resulted. This was dissolved in 5 ml 5 N HCl and heated for 60 min at 100°C in a hot aluminum block. After cooling, N_2 was bubbled through the samples for 15 min to remove volatile Br species. The solution was then diluted to exactly 2.0 N HCl (±0.1) for Se isotope analysis on the mass spectrometer.

3.3. Double isotope spike

The double spike technique has been widely used to correct for isotopic fractionation that occurs during sample preparation and mass spectrometry. It has been used for several elements, such as iron (Johnson and Beard, 1999), lead (Galer, 1999), chromium (Ellis et al., 2004), molybdenum (Siebert et al., 2001), and selenium (Johnson et al., 1999). Briefly, a double isotope spike containing ^{74}Se and ^{77}Se or ^{74}Se and ^{82}Se is introduced into each sample before purification. The $^{77}Se/^{74}Se$ or $^{82}Se/^{74}Se$ ratio of the spike is calibrated, and the measured ratio in the spike-sample mixture is later used to correct for instrumental discrimination and any isotopic fractionation during Se preparation.

3.4. Mass spectrometry and data reduction

Selenium isotope analysis was carried out on a Nu instruments HR MC-ICP-MS (Wrexham, North Wales, UK) at the Department of Geology, University of Illinois at Urbana-Champaign. Samples were introduced into the plasma as SeH_2 using a continuous flow hydride generator (HG) system described in Ellis et al. (2003) and Rouxel et al. (2002). Typical analyte is 18 ml of sample solution with 5 µg/L Se(IV). Measurements and interference corrections followed the method described in Clark and Johnson (2010). All six Se isotopes were measured simultaneously using 6 Faraday cups in static mode. The signal of ^{78}Se was 1.7–2.0 V. Signals at $m/z = 75$ and 79 were measured at the same time, to determine As and Br beam intensities. On-mass baseline measurements were made to remove Kr^+, and NiO^+ interferences and reduce $ArAr^+$ interferences. Residual $ArAr^+$ interferences at $m/z = 78$ and 76 were determined using the intensity at $m/z = 80$, and interferences from Ge^+, AsH^+, and BrH^+ were corrected for, as described in Clark and Johnson (2008).

An iterative data reduction routine (Johnson et al., 1999) was used to subtract interferences, separate the contributions from sample and spike to signals, determine mass bias, and determine the isotopic composition of samples. All Se isotopic ratios were reported relative to NIST SRM3149 in the delta notation (Carignan and Wen, 2007):

$$\delta^{82/76}\mathrm{Se} = \left[\frac{\left(\frac{^{82}\mathrm{Se}}{^{76}\mathrm{Se}}\right)_{\mathrm{sample}}}{\left(\frac{^{82}\mathrm{Se}}{^{76}\mathrm{Se}}\right)_{\mathrm{std}}} - 1\right] \times 1000 \quad (1)$$

and

$$\delta^{82/78}\mathrm{Se} = \left[\frac{\left(\frac{^{82}\mathrm{Se}}{^{78}\mathrm{Se}}\right)_{\mathrm{sample}}}{\left(\frac{^{82}\mathrm{Se}}{^{78}\mathrm{Se}}\right)_{\mathrm{std}}} - 1\right] \times 1000 \quad (2)$$

for the $^{74}Se + ^{77}Se$ double spike and

$$\delta^{78/76}\mathrm{Se} = \left[\frac{\left(\frac{^{78}\mathrm{Se}}{^{76}\mathrm{Se}}\right)_{\mathrm{sample}}}{\left(\frac{^{78}\mathrm{Se}}{^{76}\mathrm{Se}}\right)_{\mathrm{std}}} - 1\right] \times 1000 \quad (3)$$

for the $^{74}Se + ^{82}Se$ double spike. With the $^{74}Se + ^{77}Se$ double spike, the value obtained for the SRM-3149 reference solution varied with time, smoothly increasing during most analytical sessions. We attribute this to deviation of the mass bias law (Albarède and Beard, 2004) from the assumed exponential form. This causes an offset that is the

same for samples and standards. Accordingly, results are normalized to values interpolated from SRM-3149 solutions analyzed at least once per 5 samples. The $\delta^{82/78}Se$ measurements obtained with the $^{74}Se + {}^{77}Se$ double spike are partially independent of the $\delta^{82/76}Se$ measurements and are used to check for analytical errors.

3.5. Measurement reproducibility

The average $\delta^{82/76}Se$ value of 10 SRM 3149 solutions processed with TCF is $-0.024 \pm 0.08‰$ (2SD, $n = 10$). The average $\delta^{82}Se$ value of an in-house reference solution, MH495 was $-3.44 \pm 0.06‰$ (2SD, $n = 5$), in good agreement with previously published data $\delta^{82/76}Se_{MH495\ vs\ SRM3149} = -3.04 \pm 0.5‰$ from sample-standard bracketing techniques (Carignan and Wen, 2007). The same solution, when processed through the TCF sample preparation procedure, yielded an identical result ($-3.44 \pm 0.07‰$; 2SD, $n = 9$).

Duplicate digestion and analysis was carried out for 8 samples (Tables 3 and 4). Almost all of these repeated measurements yielded differences less than 0.20‰, The exceptions, YTB-fault and ytb-C, both had extremely high Se concentrations. For ytb-C, three duplicate analyses were performed. Two of the three analyses were from the same powder and the third is from a separate rock chip. $\delta^{82/76}Se$ values of the two powders are $-13.19‰$ and $-13.19‰$, respectively, while the rock chip is $-14.20‰$. The big difference (1.01‰) between them suggests that sample powder sometimes cannot be homogeneously mixed for Se-high samples that likely contain elemental Se. In light of the results from processed reference solutions and duplicate sample preparations, the external precision for $\delta^{82/76}Se$ using the $^{77}Se/^{74}Se$ spike is estimated to be $\pm 0.20‰$ (2SD, Fig. A1, Appendix). Precision for the 19 samples measured using the $^{82}Se/^{74}Se$ spike is estimated to be ± 0.12 for $\delta^{78/76}Se$, and $\pm 0.34‰$ when the results are converted to $\delta^{82/76}Se$ (Clark and Johnson, 2008).

4. RESULTS

4.1. Shadi profile

Se concentrations, $\delta^{82/76}Se$ values, and Ti concentrations are listed in Tables 1–4. The calculated mass transfer coefficient, τ, is also listed to provide an estimate of the loss or enrichment of Se due to weathering and/or Se deposition by fluids. τ is defined in the equation:

Table 1
Selenium concentrations and isotopes in rocks, efflorescent salts, and water from the Shadi profile.

Sample No.	Sample type	Se (mg/kg)	$\delta^{82/76}Se$	$\delta^{82/78}Se$	Ti (%)	t (Tau)	TOC (wt%)	TS (wt%)	Fe_2O_3 (wt%)
Upper section: strongly weathered									
SDIII-6	Shale	8.0	−1.18	−0.79	0.45	−0.99	3.38	0.13	5.52
SDIII-4	Shale	11.2	−1.21	−0.81	0.45	−0.98	2.92	0.15	5.21
SDIII-3	Shale	13.5	−1.71	−1.17	0.34	−0.97	8.26	0.21	5.57
SDIII-2	Shale	31.7	−4.08	−2.68	0.39	−0.93	8.98	3.44	3.59
SDIII-1	Shale	75.5	−1.63	−1.08	0.36	−0.83	7.55	3.48	3.35
Mean ± SD		28.0 ± 28.1	−1.96 ± 1.21	−1.31 ± 0.79		0.93 ± 0.07	6.22 ± 2.85	1.48 ± 1.81	4.65 ± 1.09
Median		13.5	−1.63	−1.08		−0.97	7.55	0.21	5.21
Middle section: some weathering apparent									
SDI-1	Shale	230	0.19	0.16	0.17	0.13	13.3	1.77	1.39
SDI-3	Chert	57.5	0.35	0.28	0.03		8.41	0.56	0.36
SDI-4	Shale	198	0.58	0.35	0.15	0.11	23.3	1.84	1.77
SDI-5	Shale	223	0.44	0.32	0.16	0.15	36.6	2.47	1.85
SDI-6	Shale	113	0.33	0.22	0.12	−0.2	18.3	1.29	1.33
SDI-7	Chert	42.2	−0.03	0.00	0.02		4.71	0.41	0.25
SDI-9	Shale	268	0.77	0.52	0.19	0.19	35.0	2.66	2.27
SDI-10	Shale	245	0.61	0.43	0.15	0.15	16.5	1.92	1.77
Mean ± SD		172 ± 88	0.41 ± 0.25	0.29 ± 0.16		0.09 ± 0.14	19.5 ± 11.6	1.62 ± 0.82	1.37 ± 0.72
Median		211	0.40	0.30		0.14	17.4	1.81	1.58
Mean (shales only)		213 ± 54	0.49 ± 0.21	0.33 ± 0.13		0.12 ± 0.14	23.8 ± 9.83	1.99 ± 0.50	1.73 ± 0.34
Median		223	0.51	0.34		0.14	20.8	1.88	1.77
Lower section: no visible weathering									
SD1	Shale	242	1.32	0.86			38.8	2.17	1.74
SD3	Shale	212	1.25	0.80	0.18	−0.02	35.5	2.12	1.57
SD4	Shale	152	1.28	0.91			26.7	1.11	0.56
SD6	Shale	233	1.38	0.98	0.16	0.21			
Mean ± SD		210 ± 40.5	1.31 ± 0.06	0.89 ± 0.08		0.10	33.7 ± 6.25	1.80 ± 0.60	1.29 ± 0.64
Median		223	1.3	0.89		0.10	35.5	2.12	1.57
Other samples									
SD5	Dolomized tuff	654	0.59	0.40			5.64	2.50	2.71
Gyp1	Gypsum	16.4	3.28	2.18					
Gyp2	Gypsum	13.1	2.95	1.95					
W1	Seep water	0.53	3.03	2.00					

Table 2
Selenium concentrations isotopes in drill cores' samples from Yutangba.

Sample	Sample type	Se (mg/kg)	$\delta^{82/76}$Se	$\delta^{82/78}$Se	$\delta^{78/76}$Se*	Depth (m)	Ti (%)	t (Tau)	TOC (wt%)	TS (wt%)	Fe_2O_3 (wt%)
Drill holes located 800 m NE of the Yutangba quarry											
Zk00B-1	Shale	110	0.71	0.46*	0.25	−27	0.10	−0.12	21.5	1.34	0.94
Zk00B-10	Shale	163	7.31	4.73*	2.56	−36	0.12	0.11	18.2	1.63	1.85
Zk00B-20	Chert	51	−0.36	−0.23*	−0.12	−41	0.072	0.30	8.42	1.22	1.44
Zk00A-38	Chert	101	0.22	0.15*	0.08	−59	0.077	1.40	6.05	1.11	1.29
Zk00A-35	Chert	104	0.26	0.17*	0.09	−63	0.14	0.39	7.89	1.66	1.36
Zk00A-30	Chert	93.5	1.70	1.10*	0.59	−65	0.065	1.63	10.0	0.98	1.40
Zk00A-25	Shale	213	1.22	0.79*	0.43	−67	0.13	0.34	16.5	1.57	1.29
Zk00A-20	Chert	84.8	1.23	0.80*	0.43	−70	0.063	1.46	9.58	1.10	1.37
Zk00A-15	Chert	119	0.58	0.38*	0.20	−73	0.092	1.37	13.4	1.28	3.15
Zk00A-11	Shale	114	0.58	0.38*	0.20	−76	0.087	0.09	21.7	1.43	1.86
Zk00A-5	Chert	73.3	−1.17	−0.76*	−0.41	−79	0.23	−0.41	10.4	3.88	3.37
Zk00A-1	Chert	22.3	−2.48	−1.61*	−0.87	−81	0.31	−0.87	3.37	3.32	4.26
Zk00C-38	Chert	113	−0.08	−0.16		−148			12.5	1.22	1.29
Zk00C-30	Shale	149	0.38	0.30		−152	0.10	0.19	22.6	3.11	2.86
Zk00C-20	Shale	150	0.60	0.37		−157	0.088	0.42	12.6	2.01	1.57
Zk00C-15	Shale	206	0.19	0.12		−161	0.17	0.02	10.1	2.05	2.74
Zk00C-8	Shale	141	0.27	0.14		−165	0.11	0.11	13.5	1.79	1.62
Zk00C-1	Chert	42.3	−1.26	−0.89		−168	0.10	−0.24	7.85	1.13	1.98
Zk00E-25	Chert	69.1	−0.54	−0.35*	−0.19	−260	0.075	0.69	9.77	2.13	1.80
Zk00E-15	Chert	35.8	0.32	0.21*	0.11	−264	0.14	−0.53	4.87	3.20	3.29
Zk00E-10	Chert	70.7	0.50	0.33*	0.18	−267	0.18	−0.26	5.17	3.70	3.09
Zk00E-1	Chert	55.9	0.47	0.31*	0.17	−274	0.29	−0.65	7.28	4.45	5.26
Drill holes located at the Yutangba quarry											
Zk180A-4	Chert	33.1	−1.07	−0.75		−58	0.27	−0.78	6.03	3.77	3.85
Zk180A-10	Chert	67.6	−1.69	−1.08		−64	0.044	1.81	8.52	1.08	1.09
Zk180A-20	Shale	150	0.07	0.05		−69	0.062	1.02	10.2	1.68	1.75
Zk180C-1	Shale	201	1.10	0.72		−126	0.093	0.80	17.0	2.02	1.72
Zk180C-5	Shale	124	0.39	0.27		−129	0.10	0.02	14.7	1.32	1.3
Zk180C-11	Shale	159	0.11	0.12		−134	0.16	−0.16	18.5	1.91	1.42
Samples from an exploration trench at the Yutangba quarry											
TC18-1	Shale	14,702	−5.35	−3.48*	−1.87	−5			14.6	1.13	1.68
Pd20-11	Shale	576	1.02	0.67*	0.36	−10			17.9	1.32	1.45
Pd16-7	Shale	494	2.24	1.46*	0.79	−21			15.8	1.03	

* Indicates measurement using $^{74}Se + {}^{82}Se$ double spike. $\delta^{82/76}$Se values were calculated from the measured $\delta^{78/76}$Se results to enable better comparisons. $\delta^{82/76}Se \approx 2.855\delta^{78/76}Se$, $\delta^{82/78}Se = [(10^3\delta^{82/76}Se) + 1/(10^3\delta^{78/76}Se + 1) - 1] \times 10^3$.

$\tau = ((C_{i,w}/C_{i,p})/(C_{j,w}/C_{j,p})) - 1$ (Brimhall et al., 1991; Scribner et al., 2006; Tuttle and Breit, 2009), where $C_{i,w}$ and $C_{i,p}$ represent the concentrations of Se in weathered and parent rock, respectively, and $C_{j,w}$ and $C_{j,p}$ are the concentrations of an inert index element in weathered and parent rock, respectively. A τ value of −1 indicates that Se has been completely lost; a value of zero indicates no loss, and a value greater than zero indicates a gain. The concentrations of Ti are roughly constant in fresh and slightly weathered samples of the Shadi and Yutangba profiles, but Ti is enriched in strongly weathered sections, consistent with the observation by Tuttle and Breit, 2009. Thus, we use Ti as the inert index component, with an assumed initial concentration of 0.13 ± 0.10 wt% (1SD, $n = 28$; median = 0.1 wt%) derived from the analyses of unaltered shale and chert from drill cores obtained at Yutangba. The average Se contents in unweathered shale and chert from drill cores are 156 ± 34 mg/kg (1SD, $n = 12$; median = 150 mg/kg) and 71.0 ± 30.0 mg/kg (1SD, $n = 16$; median = 70.0 mg/kg), respectively.

Selenium concentrations, isotopic compositions, TOC, TS, TFe and τ values from the Shadi profile are listed in Table 1 and plotted in Fig. 3A and B. Our sampling and analysis efforts at Shadi focused on shale layers; only two chert layers were analyzed. In the four shale samples from the fresh-looking rock near the base of the exposure (samples with the SD prefix), TOC is higher than strongly weathered samples, with an average of 34 ± 6.25 wt% (1SD, $n = 3$), and both TS (1.80 ± 0.60 wt%; 1SD, $n = 3$) and TFe (1.29 ± 0.64 wt%; 1SD, $n = 3$) have a significantly positive correlation (correlation coefficient $R^2 = 1$). Se concentrations varied from 152 to 242 mg/kg with an average of 210 ± 40 mg/kg (1SD, $n = 4$; median = 223 mg/kg). These concentrations are much greater than those reported for other Phanerozoic shales (Rouxel et al., 2002; Johnson and Bullen, 2004; Clark and Johnson, 2010; Mitchell et al., 2012). The $\delta^{82/76}$Se values show a very narrow range with a mean of $1.31 \pm 0.06‰$ (1SD, $n = 4$).

For the weakly weathered shales from the middle section (SDI), the two chert samples were excluded for consistency; TOC is still higher than that in strongly weathered samples, with an average of 24 ± 9.83 wt% (1SD, $n = 6$; median = 21wt%), and there is a strong positive correlation between TS (1.62 ± 0.82 wt%; 1SD, $n = 6$; median = 1.88

Table 3
Results for transects across bedding of weakly weathering (altered) rock near the base of the Yutangba quarry face.

Sample	Sample type	Se (mg/kg)	$\delta^{82/76}$Se	$\delta^{82/78}$Se	Ti (%)	*t* (Tau)	TOC (wt%)	TS (wt%)	Fe_2O_3 (wt%)	Sampling distance (cm)
Transect 1										
Cp01	Shale	2588	9.05	5.90	0.13	16	30.5	1.96	1.54	50
			8.95	5.82						
			9.13	5.94						
Cp02	Shale	2285	6.69	4.28	0.11	16	24.2	1.6	1.29	55
Cp03	Chert	2376	5.18	3.37	0.058	74	8.18	0.79	0.81	60
Cp04	Mudstone	26,054	7.88	5.13	0.22	97	17.7	1.65	3.28	65
			7.73	5.12						
Cp05	Chert	2247	5.93	3.86	0.046	88	7	0.59	0.66	70
			6.26*							
Cp06	Shale	4478	−0.68	−0.37	0.10	35	22.4	0.88	0.74	90
Cp07	Chert	1113	1.28	0.85	0.046	43	12.2	0.67	0.60	100
			1.42*							
Cp08	Chert	4873	−0.80	−0.49	0.038	23	9.82	0.53	0.49	105
			−0.64*							
Cp09	Shale	1162	5.21	3.36	0.16	5.2	39.9	2.30	1.87	113
Cp010	Chert	896	0.91	0.67	0.046	35	14.2	0.68	0.59	118
Cp011	Chert	582	−1.69	−1.04	0.022	47	8.44	0.36	0.33	126
Cp012	Chert	657	−7.91	−5.11	0.033	36	6.96	0.47	0.48	135
			−8.17*							
Cp013	Shale	1150	−8.03	−5.17	0.14	5.8	15.4	1.66	1.71	140
			−8.00	−5.17						
Cp014	Shale	396	−7.94	−5.13	0.15	1.2	26.3	0.52	0.99	151
Cp015	Mudstone	287	−1.48	−0.96	0.28	−0.2	12.1	0.31	0.88	156
Cp015a	Chert	114	2.71	1.84	0.022	8.5	2.77	0.02	0.36	166
Cp016	Shale	136	−3.76	−2.40	0.15	−0.2	25.5	0.47	0.84	170
Cp017	Chert	637	−0.78	−0.47	0.038	30	7.81	0.37	0.60	176
Cp018	Chert	316	−3.51	−2.26	0.052	10	4.67	0.38	0.50	183
Cp019	Chert	106	−0.59	−0.36	0.01	18	6.91	0.18	0.18	200
Cp020	Shale	4064	−4.10	−2.62	0.14	23	39.1	1.48	0.74	600
			−3.88*							
Cp021	Shale	1351	2.08	1.39	0.12	8.4	29.6	0.59	0.27	620
Cp021a	Mudstone	1039	−1.43	−0.93	0.35	1.5	17.0	0.44	5.26	625
Cp022	Shale	296	0.96	0.65	0.11	1.2	23.1	0.79	0.34	650
			0.87	0.61						
Transect 3										
Ytb-bottom	Shale	3254	0.13	0.08	0.44	5.16	41.23	1.74	1.76	4
Ytb-3	Shale	838	−1.45	−0.86	0.40	0.75	17.8	0.57	0.29	8
Ytb-4	Chert	1541	−2.26	−1.44	0.08	34	5.78	0.54	0.27	12
ytbA	Shale	503	−3.08	−2.01			18.8	0.71	0.4	16
Ytb-5	Shale	327	−4.51	−2.82	0.43	−0.37	46.3	1.52	0.56	20
Ytb-fault surface	Shale	1404	−6.81	−4.41	0.40	1.93	40.3	1.28	0.64	24
Ytb-B	Shale	2371	−7.29	−4.76	0.48	3.12	43.1	1.38	0.64	28
ytb-C	Shale	2622	−13.19	−8.63	0.44	3.97	40.1	2.84	1.78	32
			−13.19	−8.61						
			−14.2	−9.29						
Ytb-2	Shale	253	2.19	1.46	0.53	−0.6	44.2	1.73	0.88	36
Ytb-fault	Shale	5859	11.37	7.42	0.26	18	19.8	0.46	0.19	40
			10.39	6.74						
Ytb-1	Shale	2239	9.08	5.90	0.51	2.66	9.31	0.51	0.23	44
Si-2	Shale	1092	9.69	6.31	0.092	21	11.9	1.16	0.79	48
Si-3	Chert	4497	6.62	4.31			8.8	1	1.29	52
Si-4	Mudstone	25,472	7.03	4.58			17.3	1.48	1.63	56
			7.06	4.62						
Si-5	Chert	1181	4.88	3.17	0.089	21	4.7	0.57	0.46	60
W2	Seep water	0.43	3.23	2.11						

* Indicates measurement using $^{74}Se + {}^{82}Se$ double spike. $\delta^{82/76}$Se values were calculated from the measured $\delta^{78/76}$Se results to enable better comparisons. $\delta^{82/76}Se \approx 2.855\delta^{78/76}Se$.

Table 4
Selenium concentrations and isotopes in a transect across strongly weathered rock layers high up on the Yutangba quarry face.

Sample	Sample type	Se (mg/kg)	$\delta^{82/76}$Se	$\delta^{82/78}$Se	Ti (%)	*t* (Tau)	TOC (wt%)	TS (wt%)	Fe_2O_3 (wt%)
Transect 2									
Ytb28	Chert	119	1.98	1.33	0.21	0.04	4.45	0.21	0.94
			2.03	1.34					
Ytb27	Chert	146	−1.44	−0.92	0.22	0.22	4.75	0.18	1.47
Ytb26	Chert	17.5	−0.99	−0.63	0.16	−0.8	4.47	0.19	0.27
Ytb25	Shale	60.9	5.90	3.84	0.27	−0.81	3.67	0.10	0.26
Ytb24	Shale	4.05	1.27	0.89	0.23	−0.99	3.85	0.16	0.21
Ytb23	Shale	16.6	−1.62	−1.01	0.31	−0.96	9.79	0.27	0.37
Ytb22	Shale	30.9	−3.09	−1.99	0.033	−0.22	2.19	0.10	0.79
Ytb21	Shale	11.2	−0.63	−0.40	0.22	−0.91	5.74	0.18	
Ytb20	Shale	4.85	−0.92	−0.60	0.34	−0.99	7.50	0.25	
Ytb18	Shale	8.49	0.09	0.07	0.15	−0.95	3.77	0.19	0.57
Ytb17	Chert	4.88	−0.63	−0.37	0.02	−0.55	2.01	0.14	0.11
Ytb16	Shale	9.43	−3.54	−2.27	0.36	−0.98	6.55	0.27	0.64
Ytb15	Chert	11.7	−2.55	−1.60	0.032	−0.33	2.67	0.13	0.21
Ytb14	Shale	27.7	−2.63	−1.73	0.40	−0.94	4.24	0.24	1.12
Ytb13	Shale	5.39	−2.04	−1.29	0.32	−0.99	2.1	0.16	0.80
Ytb11	Shale	20.6	0.46	0.35	0.35	−0.95	2.25	0.23	0.93
Ytb10	Chert	8.78	3.09	2.09	0.02	−0.20	2.45	0.12	0.13
Ytb9	Shale	6.13	0.48	0.34	0.35	−0.99	1.62	0.27	0.65
Ytb7	Shale	52.2	−2.04	−1.25	0.22	−0.8	1.95	0.18	1.86
Ytb5	Shale	20.1	−4.48	−2.93	0.28	−0.94	3.05	0.15	1.74
Ytb4	Chert	4.24	-0.11	−0.06	0.13	−0.94	3.21	0.12	0.51
Ytb3	Shale	11.9	0.16	0.12	0.31	−0.97	5.05	0.18	1.19
Ytb2	Shale	1.48	0.18	0.06	0.27	−1.00	4.36	0.14	0.23
Ytb1	Shale	67.2	−2.21	−1.44	0.33	−0.83	1.30	0.11	2.63
Ytb0-C	Shale	68.4	−2.46	−1.46	0.50	−0.90	0.57	0.33	4.52
Ytb0-A	Shale	60.6	−3.42	−2.29	0.45	−0.87	3.07	0.17	1.73
Soils									
Ytb-L	Soil	19.6	−0.89	−0.50	0.31	−0.95	5.03	0.19	1.63
Ytb-L0	Soil	15.6	1.33	0.99	0.22	−0.94	3.29	0.16	1.03
Ytb-M	Soil	26.1	−3.05	−1.98	0.56	−0.96	1.43	0.12	4.51
Ytb-R	Soil	10.5	1.12	0.86	0.35	−0.98	0.67	0.14	3.22

wt%) and TFe (1.37 ± 0.72 wt%; 1SD, $n = 6$; median = 1.77 wt%) ($R^2 = 0.94$). Se concentration ranges from 113 to 268 mg/kg with an average of 213 ± 54 mg/kg (1SD, $n = 6$; median = 226 mg/kg). The average τ value is 0.12 ± 0.17 (1SD, $n = 6$). $\delta^{82/76}$Se values vary from 0.19‰ to 0.77‰ (two chert samples were −0.03 and 0.35‰). The mean $\delta^{82/76}$Se of all weakly weathered samples is 0.41 ± 0.24‰ (1SD, $n = 8$), 0.90‰ less than the mean value of the fresh-looking rocks in the lower section. For both of the fresh and weakly weathered sections, there are positive relationship between Se and TOC ($R^2 = 0.50$, $n = 11$).

In the five strongly weathered shale samples, those from the uppermost section (SDIII), TOC is heavily depleted with an average of 6.22 ± 2.85 wt% (1SD, $n = 5$; median = 7.55 wt%); TS is greatly variable from 0.13 to 3.48 wt% due to some efflorescent salts (such as gypsum) formed at the bottom of this section; TFe (4.65 ± 1.09 wt%; 1SD, $n = 5$; median = 5.21 wt%) is significantly enriched throughout SDIII section. There is a good negative correlation between TS and TFe ($R^2 = 0.98$, $n = 5$), clearly different from that in fresh-looking and weakly weathered samples. Selenium concentrations are much lower, ranging from 8.0 to 75.5 mg/kg with a mean value of 28.0 ± 28.1 mg/kg (1SD, $n = 5$; median = 13.5 mg/kg). This is approximately one seventh the concentrations of the fresh-looking samples near the base of the profile. The average τ value is -0.93 ± 0.07 (1SD, $n = 5$), indicating Se was heavily depleted. The $\delta^{82/76}$Se ranges from −1.21‰ to −4.08‰ with an average of -1.96 ± 1.08‰ (1SD, $n = 5$), 3.27‰ lower than the mean value of the fresh-looking rocks below. In comparison with the fresh and weakly weathered samples, heavy isotopes were relatively more depleted in strongly weathered samples.

Two secondary mineral samples (efflorescent salts, identified as gypsum by XRD) and one seep water sample yielded $\delta^{82/76}$Se values close to +3‰. These samples, which represent Se-enriched weathering solutions moving downward through the rock, are notably enriched in heavy isotopes compared to all rock samples in the Shadi profile. Their mean value is offset relative to fresh, slightly weathered, and strongly weathered shales by 1.8‰, 2.7‰, and 5.1‰, respectively. These results suggest that Se isotopes were fractionated during oxidative weathering of Se-rich rocks, with heavier isotopes enriched in the leachate.

4.2. Drill cores from Yutangba

The samples from Yutangba drill cores display a relatively large spread in Se concentrations, ranging from 22.3 mg/kg to 213 mg/kg (Table 2, Fig. 4). Most of this

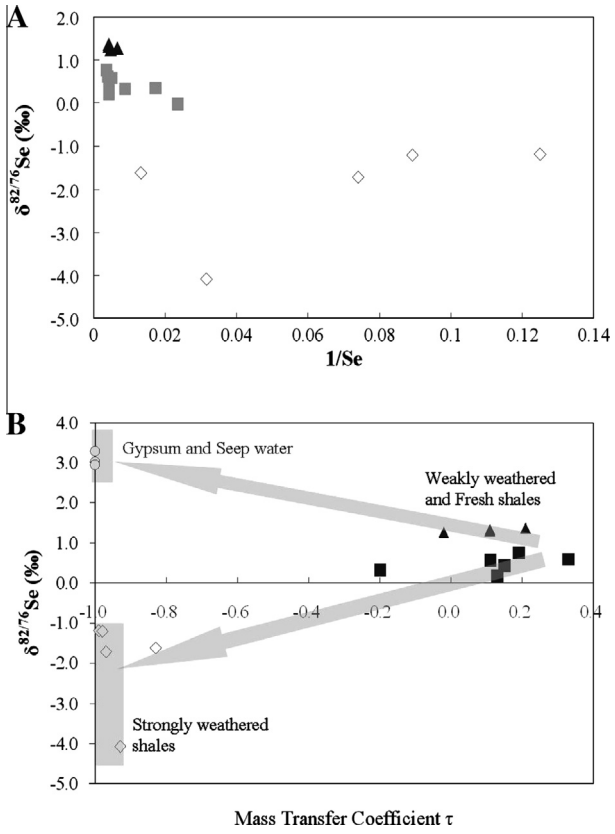

Fig. 3. (A) $\delta^{82/76}$Se vs. 1/Se (concentration) in strongly weathered to fresh shales from the Shadi outcrop. Legend: ▲ Fresh shales; ■ Weakly weathered shales; ◇ Strongly weathered shales. (B) $\delta^{82/76}$Se vs. the mass transfer coefficient (τ), an index for the extent of rock weathering. Gray arrows show the possible trend of Se isotopes evolution during oxidizing weathering. Gray boxes show the range of $\delta^{82/76}$Se in gypsum and seep water, and strongly weathered shales from Shadi.

variability is related to a systematic difference between shale and chert. The average Se concentration in shale is 156 ± 34 mg/kg (1SD, $n = 12$, median = 150), similar to that in fresh shales from Shadi, but about 2.2 times greater than that in drill core chert (71.0 ± 30.0 mg/kg; 1SD, $n = 16$, median = 70). TOC of shale and chert is 16.4 ± 4.3 wt% (1SD, $n = 12$; median = 16.7 wt%) and 8.19 ± 2.73 wt%(1SD, $n = 16$; median = 8.16 wt%), respectively, slightly lower than that in weakly weathered shales from Shadi; TS and TFe in all rocks from Yutangba drill cores are 2.04 ± 1.01 wt% (1SD, $n = 28$, median = 1.67 wt%) and 2.15 ± 1.09 wt% (1SD, $n = 28$, median = 1.74 wt%), respectively, slightly higher than those in fresh and weakly weathered shales from Shadi. These small differences may be attributed to the sampling locations and our focus only on shale layers at Shadi.

Drill core $\delta^{82/76}$Se values vary widely near the land surface but vary little at greater depth (Fig. 5; Table 2). Samples from less than 100 m depth range from −2.54 to 7.49‰ with an average of 0.49 ± 2.27‰ (1SD, $n = 15$, median = 0.27‰). Samples from deeper than 100 m have a narrower range of $\delta^{82/76}$Se, from −1.26 to 1.10‰ with an average of 0.19 ± 0.58‰ (1SD, $n = 13$, median = 0.33‰). The shale layers from the drill core have a mean $\delta^{82/76}$Se value of 0.52 ± 0.37‰ (1SD, $n = 11$, mean = 0.39‰), slightly greater than that of the chert (-0.21 ± 1.12‰; 1SD, $n = 16$, mean = 0.22‰). The overall mean $\delta^{82/76}$Se value of all drill core samples is 0.35 ± 1.69‰ (1SD, $n = 28$, median = 0.30‰), similar to that in basalt (0.35 ± 0.11‰, $n = 4$; Rouxel et al., 2002) and in other Phanerozoic shales (0.38 ± 0.47‰, 1SD, $n = 80$; Mitchell et al. (2012)). A weak correlation of $\delta^{82/76}$Se with Se concentration was observed in the Yutangba drill core (Fig. 4). The trend is defined mostly by the chert samples; some with concentrations less than about 80 mg/kg have lower $\delta^{82/76}$Se by 1–2‰.

Sample Zk00B-10, at 36 m depth, is an outlier, with a $\delta^{82/76}$Se of 7.49‰. This sample was taken close to disturbed zones interpreted to be faults (Fig. 1C). Similarly, the locations of samples Zk00A-1, Zk00A-5, Zk00C-1 and Zk180A-10 (in which TS and/or TFe are higher than other samples), were also near the inferred faults, but the $\delta^{82/76}$Se values are generally less than −1.0‰. These large isotopic contrasts suggest strong redox cycling of Se occurs along faults, which may act as conduits for relatively rapid water infiltration, possibly to depths as great as 168 m (Figs. 5 and 1C).

4.3. Weakly weathered, Se-enriched rocks from the Yutangba quarry, lower transects

Transects 1 and 3 from the Yutangba quarry combine to form a single transect of sampled rock that in hand specimen appeared to be weakly weathered. The rock is generally dark in color, having been recently excavated by local people using the rock as fertilizer. Pyrite crystals are preserved in most samples. However, iron staining and other secondary mineralization are visible on fracture surfaces. Transect 3 samples were collected at closer spacing, focused on a small area with higher Se concentrations near disturbed layering that appears to be a fault. Results are given in Table 3. For transect 1 samples, the average of TOC, TS and TFe is 17.2 ± 10.1 wt/% (1SD, $n = 23$, mean = 14.8 wt/%), 0.82 ± 0.61 wt/% (1SD, $n = 23$, mean = 0.59 wt/%), 1.06 ± 1.12 wt/% (1SD, $n = 23$, mean = 0.70 wt/%), respectively. For transect 3 samples, the average of TOC, TS and TFe is 24.6 ± 15.8 wt/% (1SD, $n = 15$, mean = 18.8 wt/%), 1.17 ± 0.65 wt/% (1SD, $n = 15$, mean = 1.16 wt/%), 0.79 ± 0.56 wt/% (1SD, $n = 15$, mean = 0.64 wt/%), respectively. These results are slightly lower than or similar to those in weakly weathered shales at Shadi. Selenium concentrations are highly variable, ranging from 106 mg/kg to 26,054 mg/kg with an average of 1441 ± 1421 mg/kg (1SD, $n = 23$, median = 1039 mg/kg) for transect 1 samples and 1971 ± 1633 mg/kg (1SD, $n = 15$, median = 1473 mg/kg) for transect 3 samples, excluding samples cp04 and Si-4, which are extremely Se-rich outliers containing approximately 3% Se, including native Se and krutaite (Zhu et al., 2004, 2012). The average τ value is 26 ± 28 (1SD, $n = 24$) in the transect 1 samples, and Se contents are approximately 8 times higher than those in fresh shale samples from Shadi and drill cores, showing a strong accumulation of Se.

The $\delta^{82/76}$Se values of samples from transect 1 range from −8.03‰ to 9.13‰; those from transect 3 range from

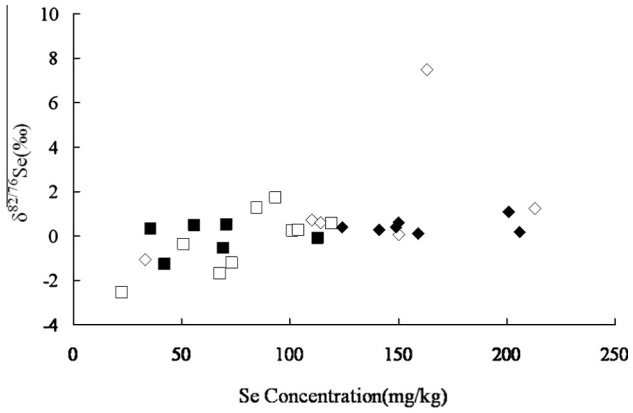

Fig. 4. $\delta^{82/76}$Se vs. Se concentration in shale and chert samples from the Yutangba drill cores only. Legend: ◇ Shallow shale; □ Shallow chert; ♦ Deep shale; ■ Deep chert.

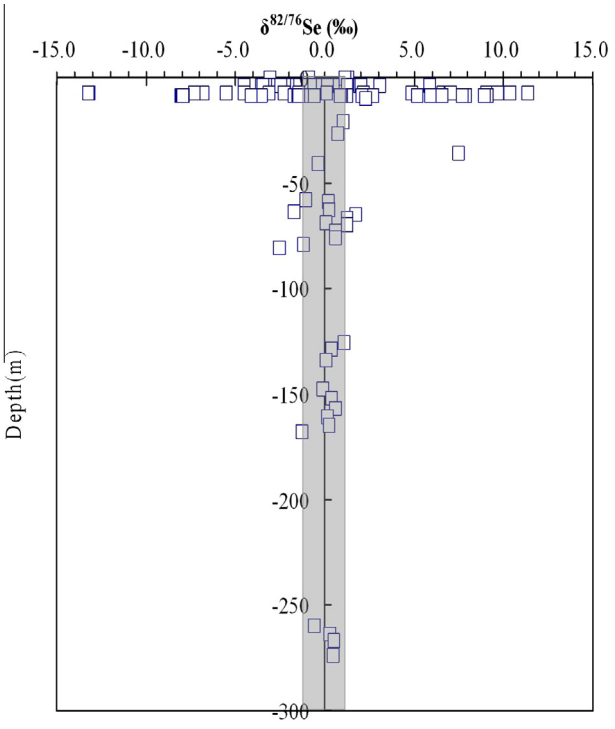

Fig. 5. $\delta^{82/76}$Se vs. depth below ground surface for all samples with sampling depth at Yutangba profile. Grey bar represents the average range (0.40 ± 0.71‰; $n = 40$) of δ^{82} Se in unweathered samples (see text) from Shadi and Yutangba.

−14.20‰ to 11.37‰ (Fig. 6). Strikingly, this range of 25.57‰ (Fig. 7), the largest Se isotopic range in any study published thus far (Rouxel et al., 2002; Johnson, 2004; Johnson and Bullen, 2004; Rouxel et al., 2004; Carignan and Wen, 2007; Clark and Johnson, 2010; Wen and Carignan, 2011) occurs over a distance of less than 10 cm (Fig. 6). An abrupt change, and the most extreme values, occurs at the location of the inferred fault. $\delta^{82/76}$Se values return to near-zero values over a distance of about 60 cm upward in the section or about 40 cm downward. These trends are mostly smooth, with little small-scale noise. The association of such strong isotopic fractionation with a fault indicates that strong redox cycling of Se was focused in the fault. However, the mean $\delta^{82/76}$Se value of the samples from transects 1 and 3 (0.45 ± 5.77‰; $n = 39$), is not strongly shifted relative to the fresh rock from deep drill core samples.

The three samples from the exploration trenches at the Yutangba quarry (a few meters deep) showed results similar to those of the samples from transects 1 and 3. Se concentrations ranged from 494 to 14702 mg/kg and $\delta^{82/76}$Se ranged from −5.48‰ to 2.30‰ (Table 2).

4.4. Strongly weathered rock from the upper part of the Yutangba quarry

Samples of strongly weathered carbonaceous shale and chert were obtained from transect 2, along the upper part of the Yutangba quarry face; sampling locations are shown in Fig 2. TOC (3.72 ± 2.05 wt/%, 1SD, $n = 26$; median = 3.44 wt/%), TS (0.18 ± 0.06 wt/%, 1SD, $n = 26$; median = 0.18 wt/%) and TFe (1.00 ± 1.00 wt/%, 1SD, $n = 26$; median = 0.72 wt/%) are much lower than those in other rocks from Yutangba drill cores and Shadi (Table 4). Selenium concentrations are highly variable, ranging from 1.14 to 146 mg/kg with an average of 30.8 ± 36.7 mg/kg (1SD, $n = 26$). These concentrations are similar to those from the highly weathered samples from Shadi, and significantly lower than those from the lower quarry transect and fresh drill core samples. The average τ value is -0.78 ± 0.35 (1SD, $n = 26$), indicating Se was strongly leached out.

$\delta^{82/76}$Se values, compared to those of the lower transect, show a somewhat narrower range between −4.48 and +3.09‰ with a mean of -0.96 ± 1.89‰ (1SD, $n = 23$), with one outlier (sample Ytb25; 5.90‰) excluded. This sample was collected from the upper part of the inferred fault near which the most extreme $\delta^{82/76}$Se values were found in the lower transects. Although the scatter is wide, the negative mean $\delta^{82/76}$Se value of transect 2 reflects a significant bias toward isotopically lighter values. This is similar to the results from the strongly weathered samples of the Shadi profile.

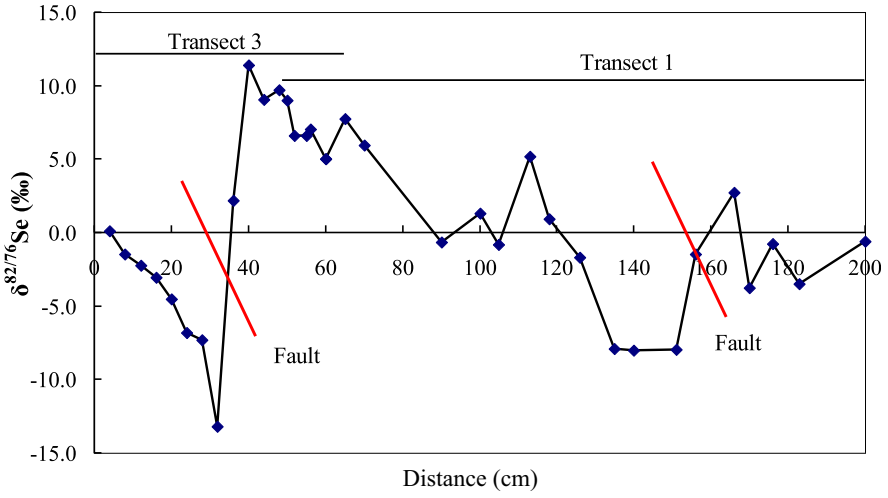

Fig. 6. $\delta^{82/76}$Se vs. distance along transects 3 and 1 across the Yutangba quarry face, as shown in Fig. 2. Here we present $\delta^{82/76}$Se values for samples collected from 2 m of transect 1 (Table 3). Red lines represent fault locations. (For interpretation of the references to color in this figure legend, the reader is referred to the web version of this article.)

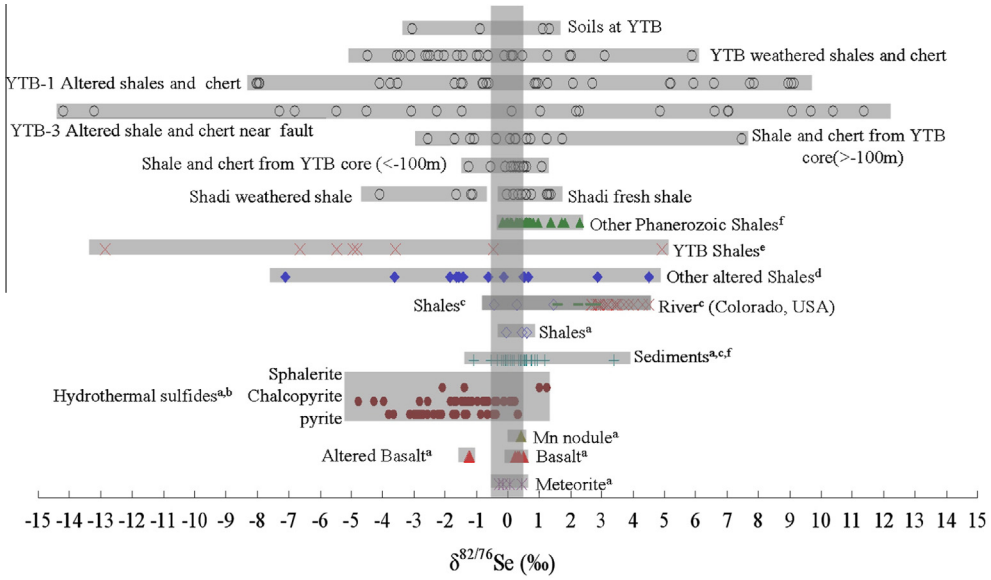

Fig. 7. Summary of Se isotopic composition of various shale samples from Shadi and Yutangba profiles, China, together with the published data in literatures. YTB-1 or 3 represents transects 1 or 3 across the Yutangba quarry face. For data in Rouxel et al.(2002, 2004), the change of scale for NIST SRM3149 was calculated using $\delta^{82/76}Se_{NIST3149} = \delta^{82/76}Se_{Spl\ vs\ Merck} + \delta^{82/76}Se_{Merck\ vs\ Nist3149} + [(^{82/76}Se_{Spl\ vs\ Merck} * \delta^{82/76}Se_{Merck\ vs\ Nist3149})/1000]$; $\delta^{82/76}Se_{Merck\ vs\ Nist3149} = 1.53‰$ (Carignan and Wen, 2007); For data in Johnson (2004), $\delta^{82/76}Se_{MH495\ vs\ Nist3149} = -3.44‰$. a: Rouxel et al. (2002); b: Rouxel et al. (2004); c: Clark and Johnson (2010); d: Johnson and Bullen (2004); e: Wen and Carignan (2011); f: Mitchell et al. (2012).

4.5. Soils from the top of the Yutangba quarry and one seepage water sample

Results from four soils at the top of the quarry face are given in Table 4. TOC (2.61 ± 1.96 wt/%, 1SD, $n = 4$; median = 2.36 wt/%) and TS (0.15 ± 0.03 wt/%, 1SD, $n = 4$; median = 0.15 wt/%) of soils are heavily depleted, while TFe (2.60 ± 1.57 wt/%, 1SD, $n = 4$; median = 2.43 wt/%) is enriched. These samples have a narrow range of Se concentration from 10.5 mg/kg to 26.1 mg/kg (17.9 ± 8.0 mg/kg, 1SD, $n = 4$; median = 17.6 mg/kg). The average τ value of Se in soils is −0.96 ± 0.02 (1SD, $n = 4$), showing that Se was almost completely leached out. $\delta^{82/76}$Se values range from −3.05‰ to 1.33‰ with a mean of -0.37 ± 2.05‰ (1SD, $n = 4$), suggesting that such moderate $\delta^{82/76}$Se variation in soils may be derived from the weathering of previously Se-rich shales with different Se isotopic composition. Notably, the mean $\delta^{82/76}$Se value

is less negative than those of the strongly weathered samples from Shadi and Yutangba.

The sample of water seeping out of the rock inside an adit cut into the Yutangba quarry face yielded a $\delta^{82/76}$Se value of 3.23‰, nearly identical to that of the water sample from Shadi.

5. DISCUSSION

5.1. Primary selenium concentrations and isotope ratios

The results clearly show that rocks from the Lower Permian Maokou Fm exposed to near-surface fluids have widely varying Se concentrations and $\delta^{82/76}$Se values; whereas rocks with less exposure are restricted to relatively narrow ranges (Fig. 7). In order to study the effects of near-surface leaching and deposition of Se, it is greatly valuable to determine the range of primary compositions prior to any alteration. However, determining the primary Se concentrations and $\delta^{82/76}$Se values of sedimentary rocks can be difficult if Se has been mobilized by reactive fluids during burial or near-surface exposure. Clearly, many of the samples studied here are highly altered, based on visual field observations and the τ values of Se (from −0.96 to 26). The obvious candidates for unaltered rocks are the deeper drill core samples from Yutangba and the fresh-looking outcrop samples from Shadi.

Drill core samples from greater than 100 m depth at Yutangba show evidence that little or no mobilization of Se has occurred. First, Se concentrations are less variable than in the near-surface regime. More importantly, $\delta^{82/76}$Se values are restricted to a narrow range (mean = 0.19‰; SD = 0.58‰; $n = 13$). This indicates that the Se redistribution processes operating in the near-surface regime (see below) have little or no impact below 100 m depth at this locality.

This near-zero $\delta^{82/76}$Se value for the primary rock coincides with results from a growing body of research on Se isotope ratios in shales and modern sediments. Mitchell et al. (2012) reported Se isotope ratios for a suite of 120 samples spanning the Phanerozoic, from Cambrian shales to modern muds. Conditions of deposition ranged from oxic to euxinic. Despite the strong contrasts in depositional setting, $\delta^{82/76}$Se values ranged only from −0.34‰ to 2.28‰, with a mean value close to zero. This stands in stark contrast to sulfur isotope ratios, which vary strongly in the same materials. Mitchell et al. (2012) concluded that the narrow $\delta^{82/76}$Se range reflected a dominance of the biological Se cycle in the oceans, with assimilation into organic matter and its eventual burial being the dominant sedimentary flux. This route of deposition involves little isotopic fractionation, whereas incorporation into sediment via dissimilatory reduction (like sulfur) would induce much larger fractionation (Johnson and Bullen, 2004; Mitchell et al., 2012). Other studies reporting Se isotope data for unaltered shales or marine sediments have also reported near-zero values (Rouxel et al., 2002; Johnson and Bullen, 2004; Clark and Johnson, 2010). Previous studies have found that organically bound Se is one of the dominant form in organic-rich sediments and shales (Kulp and Pratt, 2004; Zhu et al., 2006, 2007; Wen and Carignan, 2011). Thus, our results extend an emerging consensus that most unweathered shales have near-zero $\delta^{82/76}$Se relative to SRM-3149.

Other geochemical data support the hypothesis that Se accumulation in the Enshi sediments is driven by dissimilatory reduction and/or assimilation by marine organisms. For fresh Se-rich shales, previous studies have shown that carbonaceous shale and chert in Enshi have similar geochemical features to the Gufeng Chert on the northeastern Yangtze platform, China, with low Mn content, abundant Mo, V, Ni and Cu contents, and high organic carbon (Yao et al., 2002; Kametaka et al., 2005). This indicates both units were formed in anoxic environments during sedimentation or early digenesis. Furthermore, Se, V and Mo are all bio-essential elements and highly enriched in Se-rich shales, implying that biological activities were involved in the formation of these rocks. This is in agreement with the conclusion by Kametaka et al.(2005). Selenium is primarily accumulated in reduced fractions of shales such as organic matter and sulfides/selenides (Zhu et al., 2006, 2007; Matamoros-Veloza et al., 2011), suggesting that Se was sequestered dominantly by assimilatory biological processes with less dissimilatory reduction (Kulp and Pratt, 2004).

The visually fresh samples from the lower strata of the nearly horizontal Shadi section have mildly positive $\delta^{82/76}$Se values (mean: 1.31‰) that appear to be unaltered primary values, though this is not certain. All four samples are shale, with a narrow range of Se concentration and an extremely narrow range of $\delta^{82/76}$Se (SD: 0.05‰). Thus, there is no clear evidence of strong Se redistribution. However, it is impossible to rule out a small addition of Se to these strata via migration of Se-bearing solutions generated by weathering of overlying strata into the reducing conditions of the fresher rock. Notably, the Se concentrations of these shale samples are on average 30% greater than the unweathered shales from the Yutangba deep cores. Se added via redistribution from overlying layers could potentially cause the concentration and $\delta^{82/76}$Se difference between this rock and the deep cores, but the likelihood of this process leading to four identical $\delta^{82/76}$Se values seems remote. Thus, we tentatively classify results from these samples as unaltered primary values.

There are small, systematic differences among the $\delta^{82/76}$Se values of the unaltered samples. Among the deep Yutangba drill cores, the mean $\delta^{82/76}$Se of shale (0.52 ± 0.37‰, 1SD, $n = 11$) is greater than that of chert (-0.21 ± 1.12‰, 1SD, $n = 16$). The range of variability of the shales is very narrow, whereas the cherts exhibit greater scatter in their apparent primary compositions, with three falling within the range of the shales and three somewhat lower. In the Shadi section, similar small isotopic differences exist. The dolomized tuff layer with extremely high Se concentration, in which elemental Se reaches 20% of total Se, is closely interbeded within shales ($\delta^{82/76}$Se = 1.31 ± 0.05‰) but has a $\delta^{82/76}$Se value about 0.59‰ lower.

The Shadi section is located only 20 km from the Yutangba quarry section, and has similar thickness and rock characteristics, so the systematic $\delta^{82/76}$Se difference of 0.8‰

between the lowermost Shadi shale and unweathered Yutangba shale is unexpected. If this difference is not caused by Se redistribution in the Shadi rock as described above, it suggests variation in the marine depositional environment. Mitchell et al. (2012) ascribe similar variation in their $\delta^{82/76}$Se data set to differences in terrestrial Se input and the conditions of marine assimilation and deposition. This hypothesis could be examined further by the study of Se speciation and other geochemical proxies such as Mo isotopes.

If our assertion that the deep drill core samples from Yutangba are unaltered is correct, our observed primary Se concentrations are unusually high, being much greater than average shale (0.6 mg/kg; Turekian and Wedepohl, 1961) and Se-enriched shales of the western USA (up to 45 mg/kg; Presser et al., 1994; Kulp and Pratt, 2004). We suggest this extreme primary Se enrichment was caused by the combination of an abundant, volcanic Se source and a large flux of organic matter to the sediments. Previous studies have attributed elevated Se concentrations in the western USA to regional volcanism, with Se volatilized during eruptions later condensing and settling with ash (Floor and Román-Ross, 2011). In the Enshi case, the abundant Se probably originated from the Late Permian Emeishan large igneous province (LIP) in Southwest China (Xu et al., 2003). Some of this abundant Se was swept into a basin that was likely euxinic. TS in the fresh shales from Shadi and Yutangba is linearly related to TOC with a positive intercept on TS-axis, and TS/TOC ratio is also low (0.12 ± 0.09, $n = 29$), which can be somewhat indicative of euxinic conditions (Raiswell and Berner 1985). Significant correlations between TS and TFe in the fresh shales further indicate that both are primarily present as sulfide minerals; this further supports euxinia. The presence of pyrite nodules may strengthen that conclusion depending on their size (Wilkin et al., 1996). Thus, we suggest that an unusually large atmospheric flux of Se was transported to a local, euxinic marine basin with restricted communication with the global ocean, bio-concentrated into abundant biological materials, then deposited at the bottom of the basin to form sediment with extreme Se enrichment.

5.2. Selenium isotope shifts induced by oxidative weathering

In the strongly weathered shales and cherts at Shadi and Yutangba, Se is depleted significantly and the $\delta^{82/76}$Se of the average residual Se is shifted to negative values relative to the unaltered rock. The average $\delta^{82/76}$Se offsets relative to fresh shale are $-2.36‰$ for Shadi and $-1.48‰$ for Yutangba, with a maximum offset of $-5.46‰$. On the other hand, the seep water and efflorescent minerals, which must reflect recent seepage, have positive $\delta^{82/76}$Se values approximately 2.7‰ greater than the mean fresh rock value. These data show that Se isotopes are fractionated during oxidative weathering, presenting a systematic pattern with the heavier isotopes of Se enriched in water and depleted in the Se left behind after strong leaching. This finding is similar to the observations of Clark and Johnson (2010), who found that weathering of Mancos shale with near-zero $\delta^{82/76}$Se values produced stream waters with a mean $\delta^{82/76}$Se of $3.36 \pm 0.50‰$ (1SD, $n = 20$).

This isotopic shift might be hypothesized to result from preferential leaching of certain forms of Se from the rock. Generally, oxidative weathering of black shale involves strong decreases in both sulfides and organic matter relative to parent rocks (Littke et al., 1991; Chang and Berner, 1999; Jaffe et al., 2002; Tuttle and Breit, 2009). Because Se is dominantly associated with the organic matter and sulfide/selenides fractions in Se-rich shales (Kulp and Pratt, 2004; Zhu et al., 2006, 2007; Matamoros-Veloza et al., 2011; Qin et al., 2012), and the combination of these two fractions reaches more than 81% of total Se in our shale samples (Zhu et al., 2006), it has been suggested that oxidation of sulfides/selenides (mainly pyrite) and organic matter (OM) controls the release of Se during shale weathering (Matamoros-Veloza et al., 2011). However, pyrite oxidizes two to three orders of magnitude faster than OM during the oxidative weathering processes (Chang and Berner, 1999). We expect that sulfides/selenides should have lower $\delta^{82/76}$Se values than OM. Support for this comes from Se isotopic data in sulfides and the kerogen fraction (Rouxel et al., 2004; Wen and Carignan, 2011) and from the fact that inorganic Se(-II) is a product of dissimilatory reduction, which favors lighter isotopes (Herbel et al., 2000). Accordingly, we expect that preferential leaching of sulfide or selenide phases would remove lighter Se isotopes preferentially and leave the rock isotopically heavy. This is the opposite of our observations of strongly leached rock, seepage waters, and gypsum deposited by those waters, and we conclude that another process must dominate in fractionating Se isotopes during oxidative weathering.

Redox reactions expected to occur during the weathering process are likely to have produced the observed isotopic shifts. During progressive oxidative weathering, sulfide/selenide mineral oxidation, organic matter degradation and the formation of clay minerals and Fe/Al, Mn-oxides all occur. In strongly weathered samples, Se is mainly present as soluble Se(IV), with lesser amounts of Se(VI) and organic-Se with low molecular weight (Zhu et al., 2006, and unpublished data). There are few data on leachates, but the mobilized, soluble Se probably consists of Se(VI) and Se(IV) with lesser amounts of organically bound Se, as was observed by Clark and Johnson (2010). It is unclear if generation of Se(VI) and Se(IV) from the predominant reduced forms in the fresh rock involves any isotopic fractionation. Simple congruent dissolution would not, because this involves complete transfer of material as solids are dissolved and thus there can be no preference for either lighter or heavier isotopes.

Once the Se(VI) and Se(IV) are formed, however, they may become enriched in heavier isotopes via subsequent chemical interaction with reduced rock. Redox conditions are expected to fluctuate in much of the weathering zone: Oxidized conditions would tend to occur during influxes of water from episodic rains, whereas reducing conditions must resume as O_2 and other oxidized species are consumed during periods of stagnation. Oxidized, mobile Se formed during oxidation episodes would be subjected to re-reduction (Maes et al., 2005; Charlet et al., 2007) if it lingered in close proximity to organic-rich rock. Because reduction favors lighter isotopes, the re-reduced Se would

be enriched in lighter isotopes, creating an isotopically light precipitate and leaving the remaining dissolved, oxidized Se enriched in heavier isotopes (Johnson and Bullen, 2004). This remaining Se would then travel downward over time and may exit the Se-rich strata. In this way, we expect a general tendency for oxidized, mobile Se to develop higher $\delta^{82/76}$Se values than the primary rock. By mass balance, extensively leached rocks and those rocks in close proximity to leached horizons should have lower $\delta^{82/76}$Se values. This is the observed pattern.

Approach toward Se isotopic equilibrium could also generate the same pattern. Equilibrium exchange between oxidized Se and reduced Se results in enrichment of the oxidized Se in heavier isotopes (Li and Liu, 2011). If fluids bearing oxidized Se move into contact with rock bearing reduced Se and remain in contact for sufficient time, electron exchange reactions could result in shifts toward isotopic equilibrium. However, the rate of this process and its relative importance in nature are so far unknown. Isotopic equilibrium between Fe(III) and Fe(II) can occur rapidly (Johnson et al., 2002), but this is mostly because the Fe(III)–Fe(II) interaction is a simple one-electron exchange. Isotopic exchange for chromium, which involves transfer of three electrons between Cr(VI) and Cr(III), is very slow, with little exchange occurring over months (Zink et al., 2010). If the exchange rate for Se is fast enough to cause partial or complete isotopic equilibration during the time fluids are passing through the rock, this should lead to enrichment of oxidized, mobile Se in heavier isotopes, in addition to any enrichment occurring via partial reduction. This mechanism is similar to that proposed for copper isotope fractionation during oxidative weathering of sulfide-rich rocks (Borrok and Fernandez, 2009), in which heavier isotopes become enriched in the fluid phase via electron-exchange-driven reactions at the surface of sulfide minerals during aqueous chemical reactions.

Adsorption of Se(IV) may also be an important process in these systems. Se(IV) is more easily adsorbed by Fe/Al,Mn (hydro) oxides, clay minerals, and organic matter, relative to Se(VI) (Balistrieri and Chao, 1990; Missana et al., 2009; Wang et al., 2009). One study reported only weak isotopic fractionation between dissolved Se(IV) and Se(IV) adsorbed onto Fe(III) oxyhydroxides (Johnson et al., 1999). However, no systematic experimental data for Se isotopic fractionation associated with adsorption on organic matter, clay minerals and Fe/Al,Mn (hydro) oxides exist at this time, and this remains an open issue. Mo and U both show significant isotopic fractionation resulting from adsorption onto Mn oxides (Brennecka et al., 2011; Wasylenki et al., 2011), and Ge shows isotopic fractionation resulting from adsorption onto Fe(III) oxyhydroxides (Li and Liu, 2010). Systematic experiments of this type are needed for Se. However, adsorption of Se(IV) without a valence change likely involves little isotopic fractionation, because the bonding environment around Se(IV) would differ little between adsorbed and dissolved species (Johnson and Bullen, 2004). On the other hand, partial reduction of dissolved Se(VI) to Se(IV), or isotopic equilibration of the two species, would produce isotopically light Se(IV) while driving the remaining Se(VI) to isotopically heavy compositions. If the Se(IV) then becomes attached to the solid via adsorption, the overall result is isotopically heavy dissolved Se and a shift toward isotopically lighter rock, as we have observed.

5.3. Selenium enrichment through redox cycling

Our data suggest that Se in the Yutangba quarry has been subjected to multiple cycles of oxidation, mobilization, and re-reduction, leading to extreme Se enrichment. A recently published study (Wen and Carignan, 2011) provided an initial $\delta^{82/76}$Se data set and suggested this model for Se enrichment. Wen and Carignan (2011) analyzed a suite of nine samples from the Yutangba quarry, obtaining $\delta^{82/76}$Se values on whole rock digests and kerogen extractions. The wide range of $\delta^{82/76}$Se values we have observed was also apparent in their smaller data set. However, a strong bias toward negative $\delta^{82/76}$Se values occurring in the Wen and Carignan (2011) data set (8 out of 9 whole rock analyses are negative; mean of −4.5‰) is not borne out in our more systematic sampling (mean of 0.45‰). Their exact sample locations were not reported, but their focus was on Se ore systematics and they did not attempt to obtain a broad, unbiased sampling of the quarry rock. Overall, though, their data set show very strong Se isotope fractionation and they argued that this reflects repeated cycles of oxidation and reduction.

The regime at Yutangba may be unusual, caused by the configuration of the rock. In contrast, a simpler history for Se is consistent with the data from Shadi. In Shadi, Se mobilized by oxidation in the upper part of the outcrop can pass out of the organic-rich strata after only a few meters of seepage. The potential for repeated redox cycles is much less. However, at Yutangba, the bedding is nearly vertical (Figs. 1C and 2); waters bearing dissolved Se from the upper part of the weathering zone tend to remain within the Se-rich, organic-rich strata for tens of meters or more. The chert layers are largely impermeable and would tend to accentuate this effect by directing seepage parallel to bedding. Thus, essentially all of the Se mobilized in the oxidizing zone near the top of the system should be delivered to the underlying reducing zone, which is likely located near the water table. The Se would then be deposited there to form the current Se ore deposit, as has been suggested by Wen and Carignan (2011). Over time, as material was eroded from the top of the system, the redox front must have gradually moved deeper. As this occurred over millions of years, the Se mobilized from many meters of now-eroded rock must have become trapped in the redox front. This process, in the ore deposits literature, is known as supergene enrichment that the largest differences ($\Delta^{65}Cu_{chrysocolla\text{-}atacamite} = \sim 8‰$) in $\delta^{65/63}$Cu value were found at the Spence deposit (Palacios et al., 2011). The Se within the redox front must have been re-oxidized, mobilized, and re-reduced repeatedly, and this is consistent with the observed strong isotopic contrasts.

Although Wen and Carignan (2011) proposed supergene enrichment to explain the high Se concentrations, their data set included only nine samples, all of them from the quarry face, and thus they did not have any information about the

primary characteristics of the Maokou formation prior to near-surface alteration. Our data indicate that the primary Se concentration varies within a narrow range and that the enrichment, although spatially variable, averages about a factor of eight. Furthermore, our $\delta^{82/76}$Se data indicate that very nearly all of the >25‰ isotopic variation observed in the quarry face is not related to variation in the primary composition but rather is due to geochemical reactions occurring near the surface. This provides definitive evidence of redox involvement in the Se enrichment process.

In the fresh and weakly weathered shales from Shadi and drill cores in Yutangba (depth larger than 100 m), Selenium has a strong positive correlation with TOC and TS, and also has a significant correlation with TFe and TS. These indicate that sulfide/selenide-hosted Se (45.5% of total of Se in rock) and organically bound Se (34.3% of total of Se in rock) are dominant Se fractions. However, in the weathered shales, selenium concentration has only a weak positive correlation with TOC and TS; TFe and TS show a significant negative correlation. Organically bound Se (52.3%) is the predominant fraction. Sequential Se extractions from altered shales show that Se associated with organic matter and sulfide/selenide accounted for approximately 60% and 15% of total Se (1642 ± 1505 mg/kg), respectively (Zhu et al., 2006, 2007). This indicates that interaction of dissolved Se with organic matter also appears to play a role in trapping dissolved Se. A majority of Se occurs adsorbed by or complexed with organic matter, and a minority of Se exists as Se(-II) and Se(0). Accordingly, the mechanism by which oxidized Se is immobilized does not appear to be simple reduction to insoluble Se(0) or selenide minerals. Rather, the mobile Se reacts with organic matter to form organic-Se species. This is not unexpected; Se(IV) is known to react with thiol groups to form strong complexes (Yu et al. 1983; Rouxel et al., 2002). Thus, interaction of Se with organic matter can trap large amounts of Se as organic species in at least some parts of the system, and may play a major role in the dynamics of the weathering system.

The soil zone at the top of the Yutangba system, which has been subjected to extreme leaching, exhibits a moderate range of $\delta^{82/76}$Se (−3.05‰ to 1.33‰) with a mean value close to zero. This appears to contradict our Shadi-inspired weathering model, in which $\delta^{82/76}$Se values should tend to be negative. However, the number of soil samples from Yutangba is small, and the variation among those samples is significant. Thus, the true mean value may not be captured by these samples. Alternatively, because the soils have been subjected to intense leaching, the remaining Se is likely dominated by highly recalcitrant primary organic molecules rather than the rapidly cycled, labile Se that dominates in the redox front. Accordingly, we tentatively suggest that the processes that lead to negative $\delta^{82/76}$Se values in early weathering (see above) cease to operate under conditions of intense weathering. More work is needed to evaluate this hypothesis.

5.4. Selenium isotope systematics of redox fronts

In a redox transition zone that traps Se dissolved in downward percolating waters, certain Se isotope systematics are expected. Fluid flow pathways are complex in the Yutangba rocks, but we begin here with a simplified model of a one-dimensional system to gain general insight into expected spatial $\delta^{82/76}$Se patterns. In Fig. 8, we present a calculated model as one example of the general pattern expected at redox interfaces. We consider one-dimensional advective transport of dissolved, oxidized Se into a porous, homogenous, reducing zone. As water migrates into the reduction zone, it loses Se as it is converted to insoluble reduced Se or organic Se complexes. Se(VI) or Se(IV) reduction favors lighter isotopes (Johnson, 2004; Johnson and Bullen, 2004) and thus the remaining dissolved Se becomes progressively more enriched in the heavier isotope as the amount of Se lost increases with increasing distance traveled into the reducing zone. The $\delta^{82/76}$Se value of the reduced Se added to the rock follows that of dissolved Se, with an offset in the negative direction because of isotopic fractionation.

Importantly, the $\delta^{82/76}$Se value of the reduced and deposited Se is negative in the proximal part of the reducing zone (i.e., the part first encountered by inflowing water), and increases with increasing distance traveled into the reducing zone. It eventually becomes strongly positive in the distal part of the reducing zone, but when the water reaches there, much reduction has occurred, the dissolved Se concentration has decreased, and the amount of isotopically enriched Se deposited is also small. Accordingly, the $\delta^{82/76}$Se value in the far distal region is close to the primary value of the rock. This model is similar to the model proposed by Qi et al. (2011) of germanium isotope variation in a Ge deposit created by interaction of fluids with coal. A clear pattern in $\delta^{82/76}$Se values in the rock as a function of position occurs in this model. Rock at great depth has unaltered primary δ^{82}Se values, rock in the distal (lower) part of the reduction zone has a positive $\delta^{82/76}$Se, and rock in the proximal part has negative $\delta^{82/76}$Se.

This model is highly simplified, and the complexities of the actual system must be considered. Most importantly, flow rate in the actual system varies with position, as it is controlled by fractures in the rock and permeability differences between shale and chert layers. This is obvious, considering the extreme variations in rock Se concentration and $\delta^{82/76}$Se over short distances. However, the simple model for a homogeneous redox front can be extended to describe $\delta^{82/76}$Se variation within and near a fracture: Water flowing along a fracture into a reducing zone would evolve in essentially the same way as in the homogenous model, with the proximal part of fracture receiving isotopically lighter deposited Se and the more distal parts receiving heavier Se. Advection or diffusion of Se into rock masses adjacent to the fracture would result in a similar pattern, with rock masses immediately adjacent to the fracture receiving isotopically light Se and rock masses farther from the fracture receiving isotopically heavy Se. Based on these considerations, we suggest that rock $\delta^{82/76}$Se values are determined by the rock's accessibility to incoming water. The first reducing rock the water encounters acquires Se with lower $\delta^{82/76}$Se values. More distal rock masses acquire Se with greater $\delta^{82/76}$Se values.

Qualitatively, the pattern of $\delta^{82/76}$Se values observed in the Yutangba quarry fits this model. The material close to the inferred fault intersected by transect 3 (Fig. 2; Fig. 6)

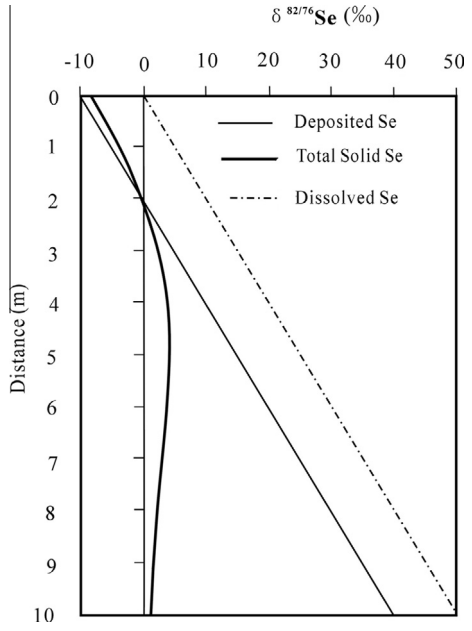

Fig. 8. A conceptual model of the spatial variation of $\delta^{82/76}$Se as a function of distance in a highly simplified, one-dimensional system with a redox front. The reducing zone begins at $z = 0$, and as water flows downward, dissolved Se is gradually lost via reduction and its $\delta^{82/76}$Se value increases. In this particular example, isotopic fractionation factor, α, is 1.010, the Se concentrations of the primary rock and the inflowing water are 10 mg/kg and 0.05 mg/L, respectively. The first-order reaction rate constant and the water velocity are chosen such that reduction removes 50% of the dissolved Se(VI) for every 1.39 m of depth, and 1000 pore volumes of water have passed through. The isotopic composition of the dissolved Se(VI) is calculated from the extent of reduction using the Rayleigh distillation equation. Qualitatively, the pattern observed here applies to any redox front: The precipitated Se causes a decrease the $\delta^{82/76}$Se value of the rock near the top of the reduction zone, but at great depth, it increases the $\delta^{82/76}$Se value. At greater depth, the rock $\delta^{82/76}$Se value approaches primary values because very little dissolved Se penetrates that far.

appears more friable and fractured than adjacent materials, and, according to observations of seepage out of the rock and visual indicators of weathering, it acts as a conduit for flow. Because this zone is quickly accessed by infiltrating water, the model predicts it should have low $\delta^{82/76}$Se. Indeed, the lowest $\delta^{82/76}$Se values from the entire site are found toward the lower side of this zone. An indication of the redox activity occurring there is the existence of abundant secondary framboidal pyrite (Fig. A2, Appendix), which is known to be produced by sulfate reducing bacteria (Wilkin et al., 1996; Donald and Southam, 1999) or abiotic redox processes (Butler and Rickard, 2000). Furthermore, because the rock layering is not vertical, we expect that some of the water passing through this zone seeps out of the fractures and downward into the underlying layers (Fig 2). The model predicts that $\delta^{82/76}$Se should increase with increasing distance downsection from the fracture; this is the pattern observed (Fig. 6). A second, less obvious fault is located at approximately 155 cm in transect 1 (Fig. 6). Here again, $\delta^{82/76}$Se values are low immediately below the fault, then increase with increasing distance downward, reaching a maximum value just above the lower fault.

Repeated redox cycling is another complicating aspect of the real system that must be considered. Most of the Se has been oxidized and re-reduced several times, as the redox front has migrated downward. Furthermore, redox conditions probably vary with changes in water influx, O_2 infiltration and/or water table elevation. During a pulse of higher flow, dissolved oxygen and other oxidants penetrate deeper and would enter the proximal parts of the reducing zone. This would cause oxidative leaching of previously deposited Se, which in the proximal zone has low $\delta^{82/76}$Se. As flow slows, Se reduction would resume, and the first Se deposited by the waters in the proximal part of the reducing zone would be shifted to lower $\delta^{82/76}$Se, relative to the already low value of the dissolved Se. The oxidized, dissolved Se that remained to migrate deeper would be shifted to greater $\delta^{82/76}$Se. In this way, repeated oxidation and reduction of Se should tend to continually drive the more accessible rock masses to isotopically light compositions, and the more distal rock masses to isotopically heavy compositions. Repeated cycling of this type would generate extreme $\delta^{82/76}$Se values, as is observed at Yutangba.

A final complicating factor is the possible presence of both dissolved Se(IV) and dissolved Se(VI) in the descending waters. Partial reduction of Se(VI) to Se(IV), or isotopic exchange between Se(IV) and Se(VI) (see above) would tend to fractionate isotopes, with the Se(VI) becoming isotopically heavier. Because Se(VI) is less prone to adsorption, it would be mobile and thus penetrate more readily to more distal or less accessible zones. This provides yet another mechanism by which spatial variation of $\delta^{82/76}$Se could be generated.

Interestingly, the average $\delta^{82/76}$Se for all samples from transects 1 and 3, despite the very strong variability, is 0.45‰ ($n = 39$), very close to the fresh shales (0.40 ± 0.71‰, 1SD, $n = 40$). Assuming transects 1 and 3 are representative of rocks in the redox front, this lack of overall isotopic shift suggests that Se accumulates in a relatively closed weathering system. Apparently, Se released from weathering in the upper parts of the system has been efficiently captured by the Yutangba reduction zone without much loss of isotopically fractionated Se.

There is no significant correlation between $\delta^{82/76}$Se and Se concentration, but samples with very high Se levels generally span a wide range of $\delta^{82/76}$Se, either more positive or negative, indicating the process causing extreme enrichment of Se is also causing the extreme $\delta^{82/76}$Se values, and that the process is closely related to Se redox transformations in this environment. As described above, repeated redox cycling probably plays a role in creating deposits of Se that are extremely fractionated isotopically, both light and heavy. However, the relationship between Se concentration and $\delta^{82/76}$Se depends on the details of redox cycling and transport, and those details are not clear to us at this point.

The restricted range of $\delta^{82/76}$Se values and the lower concentrations observed at Shadi reflect the lack of repeated redox cycling that created the Yutangba Se deposit. Because the rock layering is horizontal at Shadi, Se

mobilized by weathering can pass through the Se-rich, organic-rich strata into carbonate rocks below and is not trapped semi-permanently as it is at Yutangba. Thus, the concentration of secondary Se cannot build up to many times the primary concentration. Furthermore, repeated redox cycling of Se has not occurred to the extent it has at Yutangba, although secondary Se with variable $\delta^{82/76}$Se values probably exists within the Shadi outcrop, it is not very abundant relative to the primary Se and thus the whole-rock $\delta^{82/76}$Se variation is muted.

5.5. Implications for Se and Se isotopes in modern and ancient weathering zones

The results of this study have important implications for the general understanding of Se and Se isotopes in near-surface rocks and weathering environments. It should be expected that Se is redistributed unevenly during weathering of rocks rich in organic matter, sulfides, or other reductants. Oxidative dissolution will generate dissolved Se which may be re-deposited in underlying zones, especially if the organic-rich rock unit is thick or is steeply dipping, as in the Yutangba case. The Se deposited in these zones can be distributed unevenly, especially in shales where micro-scale permeability is very low and fluid flow is focused in fracture networks and/or faults. The isotopic composition of the deposited Se may be spatially variable, as observed in this study, with isotopically lighter Se in proximal zones and/or fractures, and isotopically heavier Se elsewhere. If the redox-driven redistribution process has operated for a long time and redox cycling of Se has been repeated many times, the magnitude of isotopic variation can be enhanced.

In light of this expected redistribution process, Se concentration and $\delta^{82/76}$Se data from outcrops, quarries and roadcuts, and even drill core from depths up to 100 m should be considered with care. In the Yutangba drill cores, significant $\delta^{82/76}$Se shifts persist to more than 80 m below the ground surface. This suggests oxidized Se penetrates to that depth. This is probably caused in part by local topographic relief of about 200 m, which should tend to drive groundwater flow to great depths. Sites with less relief may not have such deep Se redistribution.

Our results and those of Clark and Johnson (2010) suggest that dissolved Se mobilized by weathering is moderately (e.g., 3‰) enriched in heavy isotopes relative to fresh rock. If this enrichment occurs in all or most weathering zones, then riverine input to the oceans should be isotopically heavy. However, it must be noted that with sustained release of isotopically heavy Se, mass balance demands the existence of a complementary, isotopically light pool or flux of Se. Se is almost completely leached from the most weathered rock and soil at both Yutangba and Shadi, and although the highly weathered material at Shadi is isotopically light, the Se pool within it is too small and is not isotopically light enough to be the required complementary pool. In other words, if essentially all of the Se in the outcrops is eventually dissolved, it is impossible to sustain isotopically heavy leachate. Furthermore, it is possible that our four samples of seepage water and salt deposits may not be representative of the long-term weathering flux of dissolved Se. We conclude that it is possible for weathering to produce isotopically fractionated Se, but further work must be done to better understand long term, global weathering fluxes.

According to our conceptual model (above), We assert that fracture zones providing conduits for inflowing water should have lower $\delta^{82/76}$Se relative to the remainder of the rock. In the Yutangba quarry rocks, large differences in $\delta^{82/76}$Se occur over distances of only a few cm in all transects. In transect 3, only 60 cm long, extreme differences occur on this scale (Fig. 6), with the lowest $\delta^{82/76}$Se values occurring in the friable rock that has been interpreted to be a fault. The only reasonable interpretation we have found is that this feature provides an important conduit for water and the rock along the fracture thus receives Se from water that has not previously been exposed to much reduction. Further work should examine fractures and fracture zones in greater detail and determine if this phenomenon occurs universally.

6. CONCLUSIONS

Systematic variations of Se isotopic composition and concentration occur in the weathering environment of extraordinarily Se-rich carbonaceous shales and cherts of the Permian Maokou formation at Shadi and Yutangba, in Enshi prefecture, China. Nominally unaltered rock, with an average of 210 mg/kg Se, displays a narrow range of $\delta^{82/76}$Se values varying from −1.69‰ to 1.74‰ with a mean of 0.40 ± 0.71‰. This result adds to a growing body of published data indicating that shales formed at various times and in a wide range of environments tend to have near-zero values prior to near-surface alteration. The extraordinarily high primary Se concentrations in these rocks are probably related to both their extremely high organic carbon contents (3.7–46.6%), nearby volcanism in the Permian, and restricted water circulation in the basin of deposition. Minor, systematic $\delta^{82/76}$Se variations occur in the rocks, suggesting spatial and/or temporal biogeochemical variations as the rocks were deposited.

Our Se concentration and isotope results from two distinct weathering regimes reveal systematic patterns of alteration in the rock. In the Shadi section, the data reveal shifts related to degree of weathering, in sub-horizontal strata. Strongly weathered material has lost 60% to >90% of its Se; the remaining Se is isotopically light by about 3‰ relative to the fresh rock. Weakly weathered rock has lost little Se but has $\delta^{82/76}$Se values 1.7‰ less than fresh rock. Seepage waters appear to be isotopically heavy by about 1.7‰, but sampling was sparse. These data suggest that oxidative weathering preferentially removes heavy isotopes, leaving rock enriched in the lighter isotopes. It is not clear at present if this applies to other weathering environments.

The weathering regime at Yutangba, which has similar strata 20 km away from Shadi, is very different because the strata are nearly vertical. As proposed by Wen and Carignan (2011) based on a more limited data set, our results show conclusively that Se is efficiently trapped as waters seep downward and interact with the organic-rich rock. Se mobilized by oxidation becomes re-reduced and/

or adsorbed, and deposited in a redox front that has migrated downward over time, resulting in extreme Se enrichment (1642 ± 1505 mg/kg). This enrichment is accompanied by extreme isotopic contrasts, with the largest natural variations yet measured in a single study ($-14.20‰$ to $11.37‰$) occurring over distances as small as 10 cm along transects across the strata. This pattern indicates that water seepage and Se redox cycling vary strongly with position and are controlled by fractures and rock layering.

Our data and a simple conceptual model strongly suggest that, within the zone of Se deposition, zones of increased permeability that are accessed first by descending waters are isotopically light, whereas less accessible zones are heavy. Repeated redox cycling accentuates this pattern. Speculatively, we suggest that $\delta^{82/76}$Se data from organic-rich shales may provide information about relative fluid migration rates and may be useful to identify fast flow paths through the shales.

Se isotope ratios have potential as indicators of biogeochemical processes in modern environments and biogeochemical conditions over earth history, but our results suggest that primary isotopic compositions of organic-rich rocks can be significantly altered by near-surface processes. Outcrop samples can have strongly altered $\delta^{82/76}$Se values, and even apparently fresh drill core, like that from up to 80 m depth at Yutangba, may be affected. Our results also suggest that weathering tends to produce isotopically heavy dissolved Se, at least under certain circumstances. Such a shift would have implications for models of the global Se cycle and interpretation of Se isotope data from past biogeochemical regimes.

ACKNOWLEDGEMENTS

This work was supported by the National Natural Science Foundation of China (No. 41021062, 41073017), National Key Basic Research Program of China (2014CB238903), the USA National Science Foundation (EAR 07-32481 and 00-03381), and the Open Research Fund of State Key Laboratory of Ore Deposit Geochemistry, Inst. Geochemistry of CAS (No. 200912). The authors would like to thank Prof. Craig Lundstrom, Mr. Justin Glessner, Dr. Fang Huang and Dr. Zhaofeng Zhang for their assistance in sample preparation and MC-ICP-MS operation. Prof. Changxiong Liu and the No. 2 Geological Party of Hubei Province at Enshi Prefecture are also thanked for helping collect samples from drill cores and in the field. The authors also appreciate the constructive comments and suggestions of three anonymous reviewers and Dr. Marc Norman and Frederic Moynier for editorial handling.

APPENDIX A. SUPPLEMENTARY DATA

Supplementary data associated with this article can be found, in the online version, at http://dx.doi.org/10.1016/j.gca.2013.11.004.

REFERENCES

Albarède F. and Beard B. L. (2004) Analytical methods for non-traditional isotopes. In *Geochemistry of Non-Traditional Stable Isotopes* (eds. C. M. Johnson, B. L. Beard and F. Albarede). Mineralogical Society of America, Washington, pp. 113–152.

Balistrieri L. S. and Chao T. T. (1990) Adsorption of selenium by amorphous iron oxyhydroxide and manganese-dioxide. *Geochim. Cosmochim. Acta* **54**, 739–751.

Borrok D. M. and Fernandez A. (2009) Fractionation of Cu, Fe, and Zn isotopes during the oxidative weathering of sulfide-rich rocks. *Chem. Geol.* **264**, 1–12.

Brennecka G. A., Wasylenki L. E., Bargar J. R., Weyer S. and Anbar A. D. (2011) Uranium isotope fractionation during adsorption to Mn-oxyhydroxides. *Environ. Sci. Technol.* **45**, 1370–1375.

Brimhall G. H., Lewis C. J., Ford C., Bratt J., Taylor G. and Warin O. (1991) Quantitative geochemical approach to pedogenesis – Importance of parent material reduction, volumetric expansion, and eolian influx in lateritization. *Geoderma* **51**, 51–91.

Bullen T. D. and Eisenhauer A. (2009) Metal stable isotopes in low-temperature systems: A primer. *Elements* **5**, 349–352.

Bullen T. D. and Walczyk T. (2009) Environmental and biomedical applications of natural metal stable isotope variations. *Elements* **5**, 381–385.

Butler I. B. and Rickard D. (2000) Framboidal pyrite formation via the oxidation of iron(II) monosulfide by hydrogen sulphide. *Geochim. Cosmochim. Acta* **64**, 2665–2672.

Carignan J. and Wen H. J. (2007) Scaling NIST SRM 3149 for Se isotope analysis and isotopic variations of natural samples. *Chem. Geol.* **242**, 347–350.

Chang S. B. and Berner R. A. (1999) Coal weathering and the geochemical carbon cycle. *Geochim. Cosmochim. Acta* **63**, 3301–3310.

Chanton J. P., Powelson D. K., Abichou T. and Hater G. (2008) Application of nontraditional stable-isotope systems to the study of sources and fate of metals in the environment. *Environ. Sci. Technol.* **42**, 655–664.

Charlet L., Scheinost A. C., Tournassat C., Greneche J. M., Gehin A., Fernandez-Martinez A., Coudert S., Tisserand D. and Brendle J. (2007) Electron transfer at the mineral/water interface: Selenium reduction by ferrous iron sorbed on clay. *Geochim. Cosmochim. Acta* **71**, 5731–5749.

Clark S. K. and Johnson T. M. (2008) Effective isotopic fractionation factors for solute removal by reactive sediments: A laboratory microcosm and slurry study. *Environ. Sci. Technol.* **42**, 7850–7855.

Clark S. K. and Johnson T. M. (2010) Selenium stable isotope investigation into selenium biogeochemical cycling in a lacustrine environment: Sweitzer Lake, Colorado. *J. Environ. Qual.* **39**, 2200–2210.

Cutter G. A. and Bruland K. W. (1984) The marine biogeochemistry of selenium: A re-evaluation. *Limnol. Oceanog.* **29**, 1179–1192.

Cutter G. A. and Cutter L. S. (1995) Behavior of dissolved antimony, arsenic, and selenium in the Atlantic Ocean. *Mar. Chem.* **49**, 295–306.

Donald R. and Southam G. (1999) Low temperature anaerobic bacterial diagenesis of ferrous monosulfide to pyrite. *Geochim. Cosmochim. Acta* **63**(13–14), 2019–2023.

Duan Y., Anbar A. D., Arnold G. L., Lyons T. W., Gordon G. W. and Kendall B. (2010) Molybdenum isotope evidence for mild environmental oxygenation before the Great Oxidation Event. *Geochim. Cosmochim. Acta* **74**, 6655–6668.

Ellis A. S., Johnson T. M. and Bullen T. D. (2004) Using chromium stable isotope ratios to quantify Cr(VI) reduction: Lack of sorption effects. *Environ. Sci. Technol.* **38**, 3604–3607.

Ellis A. S., Johnson T. M., Herbel M. J. and Bullen T. D. (2003) Stable isotope fractionation of selenium by natural microbial consortia. *Chem. Geol.* **195**, 119–129.

Elrashidi M. A., Adriano D. C., Workman S. M. and Lindsay W. L. (1987) Chemical-equilibria of selenium in soils – A theoretical development. *Soil Sci* **144**, 141–152.

Elwaer N. and Hintelmann H. (2008) Selective separation of selenium (IV) by thiol cellulose powder and subsequent selenium isotope ratio determination using multicollector inductively coupled plasma mass spectrometry. *J. Anal. At. Spectrom.* **23**, 733–743.

Fairweather-Tait S. J., Bao Y. P., Broadley M. R., Collings R., Ford D., Hesketh J. E. and Hurst R. (2011) Selenium in human health and disease. *Antioxid. Redox Signal.* **14**, 1337–1383.

Floor G. H. and Román-Ross G. (2011) Selenium in volcanic environments: A review. *Appl. Geochem.* **27**, 517–531.

Finkelman R. B., Belkin H. E. and Zheng B. S. (1999) Health impacts of domestic coal use in China. *Proc. Natl. Acad. Sci. U.S.A.* **96**, 3427–3431.

Fordyce F. (2007) Selenium geochemistry and health. *Ambio* **36**, 94–97.

Galer S. J. G. (1999) Optimal double and triple spiking for high precision lead isotopic measurement. *Chem. Geol.* **157**, 255–274.

Hagiwara Y. (2000) Selenium isotope ratios in marine sediments and algae: A reconnaissance study. Master's thesis, University of Illinois at Urbana-Champaign, Urbana, IL.

Herbel M. J., Johnson T. M., Oremland R. S. and Bullen T. D. (2000) Fractionation of selenium isotopes during bacterial respiratory reduction of selenium oxyanions. *Geochim. Cosmochim. Acta* **64**, 3701–3709.

Herbel M. J., Johnson T. M., Tanji K. K., Gao S. D. and Bullen T. D. (2002) Selenium stable isotope ratios in California agricultural drainage water management systems. *J. Environ. Qual.* **31**, 1146–1156.

Herbel M. J., Blum J. S., Oremland R. S. and Borglin S. E. (2003) Reduction of elemental selenium to selenide: Experiments with anoxic sediments and bacteria that respire Se-oxyanions. *Geomicrobiol. J.* **20**, 587–602.

Howard H. J. (1977) Geochemistry of selenium – Formation of ferroselite and selenium behavior in vicinity of oxidizing sulfide and uranium deposits. *Geochim. Cosmochim. Acta* **41**, 1665–1678.

Jaffe L. A., Peucker-Ehrenbrink B. and Petsch S. T. (2002) Mobility of rhenium, platinum group elements and organic carbon during black shale weathering. *Earth Planet. Sci. Lett.* **198**, 339–353.

Johnson T. M. (2004) A review of mass-dependent fractionation of selenium isotopes and implications for other heavy stable isotopes. *Chem. Geol.* **204**, 201–214.

Johnson C. M. and Beard B. L. (1999) Correction of instrumentally produced mass fractionation during isotopic analysis of Fe by thermal ionization mass spectrometry. *Int. J. Mass Spectrom.* **193**, 87–99.

Johnson T. M. and Bullen T. D. (2003) Selenium isotope fractionation during reduction by Fe(II)-Fe(III) hydroxide-sulfate (green rust). *Geochim. Cosmochim. Acta* **67**, 413–419.

Johnson T. M. and Bullen T. D. (2004) Mass-dependent fractionation of selenium and chromium isotopes in low-temperature environments. *Rev. Mineral Geochem.* **55**, 289–317.

Johnson T. M., Herbel M. J., Bullen T. D. and Zawislanski P. T. (1999) Selenium isotope ratios as indicators of selenium sources and oxyanion reduction. *Geochim. Cosmochim. Acta* **63**, 2775–2783.

Johnson C. M., Skulan J. L., Beard B. L., Sun H., Nealson K. H. and Braterman P. S. (2002) Isotopic fractionation between Fe(III) and Fe(II) in aqueous solutions. *Earth Planet. Sci. Lett.* **195**, 141–153.

Kametaka M., Takebe M., Nagai H., Zhu S. and Takayanagi Y. (2005) Sedimentary environments of the Middle Permian phosphorite-chert complex from the northeastern Yangtze platform, China; the Gufeng Formation: A continental shelf radiolarian chert. *Sediment. Geol.* **174**, 197–222.

Krouse H. R. and Thode H. G. (1962) Thermodynamic properties and geochemistry of isotopic compounds of selenium. *Can. J. Chem.* **40**, 367-&.

Kulp T. R. and Pratt L. M. (2004) Speciation and weathering of selenium in Upper Cretaceous chalk and shale from South Dakota and Wyoming, USA. *Geochim. Cosmochim. Acta* **68**, 3687–3701.

Lens P. N. L. and Lenz M. (2009) The essential toxin: The changing perception of selenium in environmental sciences. *Sci. Total Environ.* **407**, 3620–3633.

Li X. F. and Liu Y. (2010) First-principles study of Ge isotope fractionation during adsorption onto Fe(III)-oxyhydroxide surfaces. *Chem. Geol.* **278**, 15–22.

Li X. F. and Liu Y. (2011) Equilibrium Se isotope fractionation parameters: A first-principles study. *Earth Planet. Sci. Lett.* **304**, 113–120.

Liang Q., Jing H. and Gregoire D. C. (2000) Determination of trace elements in granites by inductively coupled plasma mass spectrometry. *Talanta* **51**, 507–513.

Littke R., Klussmann U., Krooss B. and Leythaeuser D. (1991) Quantification of loss of calcite, pyrite, and organic-matter due to weathering of toarcian black shales and effects on kerogen and bitumen characteristics. *Geochim. Cosmochim. Acta* **55**, 3369–3378.

Maes A., Bruggeman C., Vancluysen J. and Vandenmussele P. (2005) Selenite reduction in Boom clay: Effect of FeS2, clay minerals and dissolved organic matter. *Environ. Pollut.* **137**, 209–221.

Marin L., Lhomme J. and Carignan J. (2001) Determination of selenium concentration in sixty five reference materials for geochemical analysis by GFAAS after separation with thiol cotton. *Geostand. Newsl.* **25**, 317–324.

Matamoros-Veloza A., Newton R. J. and Benning L. G. (2011) What controls selenium release during shale weathering? *Appl. Geochem.* **26**(Suppl.), s222–s226.

Missana T., Alonso U. and Garcia-Gutierrez M. (2009) Experimental study and modelling of selenite sorption onto illite and smectite clays. *J. Colloid Interface Sci.* **334**, 132–138.

Mitchell K., Mason P. R. D., Van Cappellen P., Johnson T. M., Gill B. C., Owens J. D., Diaz J., Ingall E. D., Reichart G.-J. and Lyons T. W. (2012) Selenium as paleo-oceanographic proxy: A first assessment. *Geochim. Cosmochim. Acta* **89**, 302–317.

Nelson D. C., Casey W. H., Sison J. D., Mack E. E., Ahmad A. and Pollack J. S. (1996) Selenium uptake by sulfur-accumulating bacteria. *Geochim. Cosmochim. Acta* **60**, 3531–3539.

Palacios C., Rouxel O., Reith M., Cameron E. M. and Leybourne M. I. (2011) Pleitocene recycling of copper at a prophyry system, Atacama Desert, Chile: Cu isotope evidence. *Miner Deposita* **46**, 1–7.

Pearce C. R., Burton K. W., Pogge von Strandmann P. A. E., James R. H. and Gislason S. R. (2010) Molybdenum isotope behaviour accompanying weathering and riverine transport in a basaltic terrain. *Earth Planet. Sci. Lett.* **295**, 104–114.

Presser T. S., Sylvester M. A. and Low W. H. (1994) Bioaccumulation of selenium from natural geologic sources in western states and its potential consequences. *Environ. Manage.* **18**, 423–436.

Qi H. W., Rouxel O., Hu R. Z., Bi X. W. and Wen H. J. (2011) Germanium isotopic systematics in Ge-rich coal from the Lincang Ge deposit, Yunnan, Southwestern China. *Chem. Geol.* **286**, 252–265.

Qin H. B., Zhu J. M. and Su H. (2012) Selenium fractions in organic matter from Se-rich soils and weathered stone coal in selenosis areas of China. *Chemosphere* **86**, 626–633.

Raiswell R. and Berner R. A. (1985) Pyrite formation in euxinic and semi-euxinic sediments. *Am. J. Sci.* **285**, 710–724.

Rayman M. P. (2000) The importance of selenium to human health. *Lancet* **356**, 233–241.

Rees C. E. and Thode H. G. (1966) Selenium isotope effects in reduction of sodium selenite and of sodium selenate. *Can. J. Chem.* **44**, 419–421.

Rouxel O., Ludden J., Carignan J., Marin L. and Fouquet Y. (2002) Natural variations of Se isotopic composition determined by hydride generation multiple collector inductively coupled plasma mass spectrometry. *Geochim. Cosmochim. Acta* **66**, 3191–3199.

Rouxel O., Fouquet Y. and Ludden J. N. (2004) Subsurface processes at the Lucky Strike hydrothermal field, Mid-Atlantic Ridge: Evidence from sulfur, selenium, and iron isotopes. *Geochim. Cosmochim. Acta* **68**, 2295–2311.

Schilling K., Johnson T. M. and Wilcke W. (2011) Isotope fractionation of selenium during fungal biomethylation by *Alternaria alternata*. *Environ. Sci. Technol.* **45**, 2670–2676.

Scribner A. M., Kurtz A. C. and Chadwick O. A. (2006) Germanium sequestration by soil: Targeting the roles of secondary clays and Fe-oxyhydroxides. *Earth Planet. Sci. Lett.* **243**, 760–770.

Seby F., Potin-Gautier M., Giffaut E., Borge G. and Donard O. F. X. (2001) A critical review of thermodynamic data for selenium species at 25 degrees C. *Chem. Geol.* **171**, 173–194.

Siebert C., Nagler T. F. and Kramers J. D. (2001) Determination of molybdenum isotope fractionation by double-spike multicollector inductively coupled plasma mass spectrometry. *Geochem. Geophy. Geosy.* **2**, paper number 2000GC000124.

Song C. Z. (1989) A brief description of the Yutangba sedimentary type Se mineralized area in outhwestern Hubei. *Miner. Deposits* **8**, 83–88 (in Chinese with English Abstract).

Stolz J. E., Basu P., Santini J. M. and Oremland R. S. (2006) Arsenic and selenium in microbial metabolismSong, C.Z., A brief description of the Yutangba sedimentary type Se mineralized area in outhwestern Hubei, Miner. Deposits 8, 1989, 83-88, (in Chinese with English Abstract). *Annu. Rev. Microbiol.* **60**, 107–130.

Tan J. A., Zhu W. Y., Wang W. Y., Li R. B., Hou S. F., Wang D. C. and Yang L. S. (2002) Selenium in soil and endemic diseases in China. *Sci. Total Environ.* **284**, 227–235.

Teng F. Z., Li W. Y., Rudnick R. L. and Gardner L. R. (2010) Contrasting lithium and magnesium isotope fractionation during continental weathering. *Earth Planet. Sci. Lett.* **300**, 63–71.

Turekian K. and Wedepohl K. H. (1961) Distribution of the elements in some major units of the earth's crust. *Geol. Soc. Amer. Bull.* **72**, 175–192.

Tuttle M. L. W. and Breit G. N. (2009) Weathering of the New Albany Shale, Kentucky, USA: I. Weathering zones defined by mineralogy and major-element composition. *Appl. Geochem.* **24**, 1549–1564.

Wang H. F. and Li J. Q. (1996) Geological characteristics of selenium ore deposit in Shuanghe, Enshi, Hubei Province. *Hubei Geol.* **10**, 10–21 (in Chinese with English Abstract).

Wang M. K., Chan Y. T., Kuan W. H. and Chen T. Y. (2009) Adsorption mechanism of selenate and selenite on the binary oxide systems. *Water Res.* **43**, 4412–4420.

Wasylenki L. E., Weeks C. L., Bargar J. R., Spiro T. G., Hein J. R. and Anbar A. D. (2011) The molecular mechanism of Mo isotope fractionation during adsorption to birnessite. *Geochim. Cosmochim. Acta* **75**, 5019–5031.

Wen H. J. and Carignan J. (2011) Selenium isotopes trace the source and redox processes in the black shale-hosted Se-rich deposits in China. *Geochim. Cosmochim. Acta* **75**, 1411–1427.

World Health Organization (WHO) (1987) Environmental Health Criteria 58: Selenium Environmental Health Criteria. *Geneva*, 1–110.

Wilkin R. T., Barnes H. L. and Brantley S. L. (1996) The size distribution of framboidal pyrite in modern sediments: An indicator of redox conditions. *Geochim. Cosmochim. Acta* **60**(20), 3897–3912.

Williams P. N., Lombi E., Sun G. X., Scheckel K., Zhu Y. G., Feng X. B., Zhu J. M., Carey A. M., Adomako E., Lawgali Y., Deacon C. and Meharg A. A. (2009) Selenium characterization in the global rice supply chain. *Environ. Sci. Technol.* **43**, 6024–6030.

Xu Y. G., He B., Chung S. L., Xiao L. and Wang Y. (2003) Sedimentary evidence for a rapid, kilometer-scale crustal doming prior to the eruption of the Emeishan flood basalts. *Earth Planet. Sci. Lett.* **213**, 391–405.

Yang G. Q., Wang S. Z., Zhou R. H. and Sun S. Z. (1983) Endemic selenium intoxication of humans in China. *Am. J. Clin. Nutr.* **37**, 872–881.

Yao L. B., Gao Z. M., Yang Z. S. and Long H. B. (2002) Origin of seleniferous cherts in Yutangba Se deposit, southwest Enshi, Hubei Province. *Sci. China Ser. D* **45**, 741–754.

Yu M.-Q., Liu G.-Q. and Jin Q. (1983) Determination of trace arsenic, antimony, selenium and tellurium in various oxidation states in water by hydride generation and atomic-absorption spectrophotometry after enrichment and separation with thiol cotton. *Talanta* **30**, 265–270.

Zheng B. S., Ding Z. H., Huang R. G., Zhu J. M., Yu X. Y., Wang A. M., Zhou D. X., Mao D. J. and Su H. C. (1999) Issues of health and disease relating to coal use in southwestern China. *Int. J. Coal Geol.* **40**, 119–132.

Zhu J. M., Zuo W., Liang X. B., Li S. H. and Zheng B. S. (2004) Occurrence of native selenium in Yutangba and its environmental implications. *Appl. Geochem.* **19**, 461–467.

Zhu J. M., Qin H. B., Luo T. Y., Li L. and Su H. C. (2007) A comparative study of selenium fractionation in Se-rich carbonaceous rocks of Lower Cambrian and Permian in Southwest China. *Geol. J. China Univ.* **13**, 69–74 (in Chinese with English abstract).

Zhu J. M., Han W. L., Lei L. and Zhao Y. Z. (2006) Selenium speciation of Se-rich rocks from Yutangba of Enshi, China. *Geochim. Cosmochim. Acta* **70**. A754.

Zhu J. M., Johnson T. M., Clark S. K. and Zhu X. K. (2008a) High precision measurement of selenium isotopic composition by hydride generation multiple collector inductively coupled plasma mass spectrometry with a Se-74-Se-77 double spike. *Chin. J. Anal. Chem.* **36**, 1385–1390.

Zhu J. M., Wang N., Li S., Li L., Su H. and Liu C. X. (2008b) Distribution and transport of selenium in Yutangba, China: Impact of human activities. *Sci. Total Environ.* **392**, 252–261.

Zhu J. M., Johnson T. M., Finkelman R. B., Zheng B. S., Sykorova I. and Pesek J. (2012) The occurrence and origin of selenium minerals in Se-rich stone coals, spoils and their adjacent soils in Yutangba. *China. Chem. Geol.* **330–331**, 27–38.

Zhu Y. G., Pilon-Smits E. A. H., Zhao F. J., Williams P. N. and Meharg A. A. (2009) Selenium in higher plants: understanding mechanisms for biofortification and phytoremediation. *Trends Plant Sci.* **14**, 436–442.

Zink S., Schoenberg R. and Staubwasser M. (2010) Isotopic fractionation and reaction kinetics between Cr(III) and Cr(VI) in aqueous media. *Geochim. Cosmochim. Acta* **74**(20), 5729–5745.

Associate editor: Frederic Moynier